

Stability of bounded rapid shear flows of a granular material

By CHI-HWA WANG, R. JACKSON AND S. SUNDARESAN

Department of Chemical Engineering, Princeton University, Princeton, NJ 08544, USA

(Received 24 November 1994 and in revised form 6 June 1995)

This paper presents a linear stability analysis of a rapidly sheared layer of granular material confined between two parallel solid plates. The form of the steady base-state solution depends on the nature of the interaction between the material and the bounding plates and three cases are considered, in which the boundaries act as sources or sinks of pseudo-thermal energy, or merely confine the material while leaving the velocity profile linear, as in unbounded shear. The stability analysis is conventional, though complicated, and the results are similar in all cases. For given physical properties of the particles and the bounding plates it is found that the condition of marginal stability depends only on the separation between the plates and the mean bulk density of the particulate material contained between them. The system is stable when the thickness of the layer is sufficiently small, but if the thickness is increased it becomes unstable, and initially the fastest growing mode is analogous to modes of the corresponding unbounded problem. However, with a further increase in thickness a new mode becomes dominant and this is of an unusual type, with no analogue in the case of unbounded shear. The growth rate of this mode passes through a maximum at a certain value of the thickness of the sheared layer, at which point it grows much faster than any mode that could be shared with the unbounded problem. The growth rate of the dominant mode also depends on the bulk density of the material, and is greatest when this is neither very large nor very small.

1. Introduction

Several years ago, in a computer simulation of plane shearing motion of an assembly of smooth inelastic disks, Hopkins & Louge (1991) observed the development of a dynamic structure consisting of an anisotropic distribution of clusters of increased particle concentration, indicating that the initially uniform random distribution of particles was unstable under shear. Since that time other simulations have demonstrated similar clustering tendencies (see, for example, Goldhirsch, Tan & Zanetti 1993), and these results raise the question of the stability of plane shear, regarded as a steady solution of macroscopic continuum equations of motion for a granular material, such as those formulated by Haff (1983), Jenkins & Savage (1983), Lun *et al.* (1984) and Jenkins (1987), and subsequently elaborated and generalized by a number of workers. An early investigation by Mello, Diamond & Levine (1991) of disturbance propagation about a plane shearing motion, based on the continuum equations derived from granular kinetic theory, bypassed the essentials of the stability problem by confining attention to disturbances with wave vectors in the direction of the vorticity. (However, these authors did briefly examine the stability problem for the more complicated Taylor–Couette flow.) Both McNamara (1993) and Goldhirsch *et al.* (1993), on the other hand, used the continuum equations to investigate the stability of

a uniform granular material during ‘cooling’ due to the loss of pseudo-thermal energy in inelastic collisions and McNamara also examined the stability of a granular material maintained at a steady state by a uniformly distributed source of pseudo-thermal energy.

The first systematic attempt to investigate the stability of the solution of the continuum equations representing an infinite plane shearing motion was made by Savage (1992). When these equations are linearized about the base state, $\mathbf{u}_0 = (\Gamma y, 0, 0)$, the coefficients of certain terms are found to be functions of y as a result of the dependence of $u_{0,x}$ on y , and this precludes the existence of simple harmonic wave solutions. Consequently, Savage adopted a procedure used by Moffat (1967) in which solutions of the linearized equations are sought in the form

$$\mathbf{a}(x, y, t) = \mathbf{a}(t) \exp[i\mathbf{k}(t) \cdot \mathbf{x}], \quad (1)$$

where $\mathbf{k}(t) = [k_x, k_y] = [k_x^0, k_y^0 - \Gamma t k_x^0]$ and \mathbf{a} represents the vector of dependent variables, namely the volume fraction of solids, the two components of velocity, and the granular temperature. k_x^0 and k_y^0 are constant wavenumbers associated with the x - and y -directions, respectively, and (1) represents plane waves whose wavefronts rotate in conformity with the vorticity of the base-state flow field. (Modes of this type were originally introduced by W. Thomson, later Lord Kelvin, in a study of the stability of bounded plane shear for a Newtonian fluid (Thomson 1887), so they will be referred to as ‘Kelvin modes’ in what follows.) With this substitution the linearized perturbation equations reduce to linear ordinary differential equations, with time-dependent coefficients, for the components of $\mathbf{a}(t)$. In the simpler case of a shearing Newtonian fluid Thomson (and Moffat) found explicit solutions of these equations but, as this was not possible for the corresponding but more complicated equations for granular materials, Savage replaced the time-dependent coefficients in the equations for \mathbf{a} by constants, equal to their values at $t = 0$. The resulting equations then had solutions of the form (1), but with $\mathbf{k}(t)$ replaced by a constant wave vector $\mathbf{k}(0)$, and $\mathbf{a} = \mathbf{a}(0) \exp(\omega t)$. These satisfied the complete differential equations for $\mathbf{a}(t)$ exactly only at $t = 0$, and presumably approximated the solution of these equations for sufficiently small values of t . Savage then classified the base state as stable if the real part of ω was negative for all solutions of this type, and unstable if it was positive for any solution. The largest real part of ω , which will be referred to as the initial growth rate, was also presented graphically as a function of k_y^0 , for various fixed values of k_x^0 and various base states. It was found that the base states examined were unstable, in the above sense, with the initial growth most rapid when the two components of the wavenumber vector were approximately equal. The initial growth rates were also found to be larger for intermediate values of the solids volume fraction, rather than very large or small values.

Following a procedure mathematically identical with that of Savage, Babić (1993) later presented a more extensive set of results, with the dependence of the initial growth rate on k_x^0 and k_y^0 exhibited graphically as contour plots for fixed values of the solids volume fraction ν_0 in the base state. Babić also considered the effect of permitting the wave vector to have a non-vanishing component k_z^0 in the direction of the vorticity.

A difficulty with the results of Savage and of Babić is that the existence of small perturbations which grow initially does not, in itself, imply that the base state is unstable, in the conventional sense. Recalling the definitions of stability and asymptotic stability, in the sense of Lyapunov, a transient perturbation solution of the linearized equations which remains bounded for all $t \geq 0$ cannot provide evidence of instability of the base state, since it remains a solution when multiplied by any scale factor. Thus,

it can be constrained to remain within any specific bounds, no matter how small, simply by scaling down the initial perturbation, and this meets the Lyapunov definition of stability. Furthermore if, in addition, it tends to zero as t tends to infinity, then it also meets the definition of asymptotic stability. The value of the initial rate of change or, indeed, the largest value attained by the transient (provided this remains bounded) is not related to the question of instability, in the Lyapunov sense. In the cases they identify as ‘unstable’ the solutions of Savage and of Babić increase without bound when $t \rightarrow \infty$, but this is of no relevance, since they approximate the solution of the complete differential equations for $\mathbf{a}(t)$ only for small values of t . This was recognized by Babić, who qualified the presentation of his results in the following words: “in the subsequent presentation the disturbance growth will be referred to as ‘instability’, although the initial exponential growth does not imply exponential growth at all times”.

The relation of the Kelvin modes to the question of stability has subsequently been clarified significantly by the work of Schmid & Kytömaa (1994). These authors considered both the complete differential equations for $\mathbf{a}(t)$, with time-variable coefficients, and the form to which these are reduced by the above device of replacing the variable coefficients by constants equal to their initial values. They were able to calculate the following function of time:

$$G(t) = \sup_{\mathbf{a}(0) \neq 0} \frac{\|\mathbf{a}(t)\|}{\|\mathbf{a}(0)\|},$$

where $\|\mathbf{a}\|$ denotes the norm of \mathbf{a} , defined as the sum of the squares of its components. This function is then an envelope for the norms of all possible transient solutions, scaled so that their initial conditions have unit norm. In this way they were able to show that solutions of the differential equations with constant coefficients could have initial rates of increase considerably larger than those corresponding to the separate exponentially growing modes investigated by Savage and Babić, so the initial growth rates reported by these authors are not even a reliable guide to the short-time behaviour of small disturbances. Also illuminating are calculations of $G(t)$ for solutions of the complete differential equations for $\mathbf{a}(t)$, whose coefficients have a quadratic dependence on time. Then it is found that G may increase rapidly for small values of t and attain a large maximum value for certain ranges of k_x^0 and k_y^0 . Nevertheless, when $k_x^0 \neq 0$ they are able to show that $G(t)$ always tends to zero as $t \rightarrow \infty$. Thus, transient solutions of the Kelvin form (1), with $k_x^0 \neq 0$, remain bounded for all t and tend to zero as t tends to infinity, so none of them represents instability, in the sense of Lyapunov. Unfortunately this does not imply the converse, that the base state is stable in the sense of Lyapunov, since there remain the Kelvin modes with $k_x^0 = 0$, which we will return to below, and there may also be other solutions of the linearized equations of motion which are not of the Kelvin form. Schmid & Kytömaa also point out that the large amplification of initial conditions at some finite value of the time may be of concern, since it could trigger unstable behaviour associated with the nonlinearities of the equations of motion. Of course this could always be avoided by constraining the initial disturbances to be sufficiently small, but it indicates that the base state, even if formally stable in the sense of Lyapunov, might have a very circumscribed domain of attraction. Furthermore, even if no instability is triggered, the base state might be expected to be subject to significant fluctuations as a result of transient magnification of small random perturbations.

For the Kelvin modes with $k_x^0 = 0$, and only for these, the differential equations satisfied by the components of $\mathbf{a}(t)$ have constant coefficients, so the results obtained

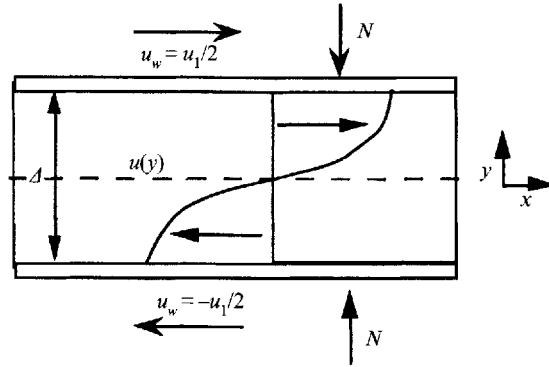


FIGURE 1. Bounded plane shear flow. N denotes normal stress confining the plates. u_w is the speed of the plates.

by Savage, and by Babić, are true solutions of the complete equations, valid for all times. The growth rates of these modes as a function of k_y^0 , as plotted by Savage (1992) for two different base states, appear to be less than or equal to zero. However, for a base-state solids volume fraction of 0.3, the computed growth rates are actually positive over a limited range of values of k_y^0 , though they are too small to be seen on the scale of the figures. (We are indebted to Professor Savage for providing us with his computed results, which are in agreement with independent calculations in the present work.) The existence of these exponentially growing modes is sufficient to establish that the corresponding base states are truly unstable, in the sense of Lyapunov, and the instability takes the form of alternating layers of higher and lower particle concentration oriented parallel to the planes of shear. (The corresponding growth rates, are, however, much slower than the largest initial growth rates for the rotating Kelvin modes with $k_x^0 \neq 0$.) We shall refer to these modes in what follows as *layering modes*. Examination of Babić's growth rate contour plots reveals the same feature, for particles both in the form of spheres and two-dimensional disks. The 'unstable' domain enclosed by the 'neutral stability' contour includes an interval of the $k_x^0 = 0$ axis containing the origin, and points on this interval (other than the origin itself) represents truly unstable behaviour in the Lyapunov sense though, as noted above, no such behaviour is found anywhere else in the (k_x^0, k_y^0) -plane.

The above considerations are discussed clearly, and at some length, in Appendix A of the recent paper by McNamara (1993). However, McNamara invokes Schmid & Kytömaa's result on the asymptotic decay of the Kelvin modes to conclude, incorrectly, that unbounded plane shear of a granular material is always linearly stable. The fallacy lies in failing to recognize that Schmid & Kytömaa's result holds only for $k_x \neq 0$. As pointed out above, there are cases where linearly unstable modes exist with $k_x = 0$, so the unbounded plane shear is linearly unstable.

In the present paper we focus attention on the stability of a shearing layer of finite thickness, bounded by rigid impenetrable walls at $y = \pm D/2$ (see figure 1). In hydrodynamic stability problems in general it is found that the presence of solid boundaries has a profound effect on the stability of the flow, and we shall show that this is also the case for this problem. First we note that the ambiguities associated with the Kelvin modes for $k_x^0 \neq 0$, discussed at some length above, are not of concern for the bounded problem, since these modes are incompatible with the requirement that the boundaries shall be everywhere impenetrable to the particles. Certain layering modes with $k_x^0 = 0$, on the other hand, are consistent with the condition of

impenetrability, and we shall see that they contribute part of the stability picture for the bounded problem. However, they are by no means the most significant part of this picture. We shall show that the strongest modes of unstable behaviour found for the bounded problem are of a new and unexpected type, with no analogue in the unbounded problem. Thus, the presence of the bounding walls induces a physically new type of behaviour.

2. Governing equations

Solutions for steady plane shearing of a granular material between parallel plates, valid in the ‘rapid flow’ regime, have been generated numerically by Johnson & Jackson (1987), using the form of equations proposed for this regime by Lun *et al.* (1984). To maintain consistency with this earlier work, and with more recent work on the stability of unbounded plane shear flow (Savage 1992; Babić 1993; Schmid & Kytömaa 1994), the same equations are adopted here, and will now be summarized for convenience. There are three equations, representing conservation of material, momentum and the pseudo-thermal energy associated with fluctuations of particle velocities about the mean, respectively. In the absence of gravity they take the form

$$\frac{\partial \rho}{\partial t} + \nabla \cdot (\rho \mathbf{u}) = 0, \quad (2)$$

$$\rho \frac{D\mathbf{u}}{Dt} = -\nabla \cdot \boldsymbol{\sigma}, \quad (3)$$

$$\frac{3}{2}\rho \frac{DT}{Dt} = -\nabla \cdot \mathbf{q} - \boldsymbol{\sigma} : \nabla \mathbf{u} - J. \quad (4)$$

Here ρ is the bulk density of the material, given by $\rho = \rho_p \nu$, where ν is the volume fraction of solids and ρ_p the density of the solid material; \mathbf{u} is the local value of the mean velocity; $\boldsymbol{\sigma}$ is the stress tensor, defined in the compressive sense; and T is the grain temperature, defined as $\frac{1}{3}\langle u'^2 \rangle$, where u' is the magnitude of the fluctuation about the local mean velocity; \mathbf{q} is the flux vector of the pseudo-thermal energy, identified as the mean kinetic energy of the velocity fluctuations; and J denotes the rate of dissipation of this energy, per unit volume, as a consequence of the inelasticity of collisions between particles. D/Dt represents the material time derivative following the mean motion.

In the absence of frictional contributions to the stress, following Lun *et al.* (1984), the following closures are adopted for $\boldsymbol{\sigma}$, \mathbf{q} and J :

$$\boldsymbol{\sigma} = [\rho T(1 + 4\eta \nu g_0) - \eta \mu_b \nabla \cdot \mathbf{u}] \mathbf{I} - \left(\frac{2 + \alpha}{3} \right) \left\{ \frac{2\mu}{\eta(2 - \eta)g_0} (1 + \frac{8}{5}\nu \eta g_0) [1 + \frac{8}{5}\eta(3\eta - 2)\nu g_0] + \frac{6}{5}\eta \mu_b \right\} \mathbf{S}, \quad (5)$$

$$\mathbf{q} = -\frac{\lambda}{g_0} \left\{ (1 + \frac{12}{5}\eta \nu g_0) [1 + \frac{12}{5}\eta^2(4\eta - 3)\nu g_0] + \frac{64}{25\pi} (41 - 33\eta)(\eta \nu g_0)^2 \right\} \nabla T - \frac{\lambda}{g_0} \frac{12}{5} \eta(\eta - 1)(2\eta - 1) [1 + \frac{12}{5}\eta \nu g_0] \frac{d}{dy} (\nu^2 g_0) \frac{T}{\nu} \nabla \nu, \quad (6)$$

$$J = \frac{48}{\pi^{1/2}} \eta(1 - \eta) \frac{\rho_p \nu^2}{d} g_0 T^{3/2}, \quad (7)$$

where \mathbf{S} is the deviatoric part of the rate of deformation:

$$\mathbf{S} = \frac{1}{2}(\nabla\mathbf{u} + \nabla\mathbf{u}^T) - \frac{1}{3}\nabla \cdot \mathbf{u}\mathbf{I}.$$

η is related to the coefficient of restitution, e_p , for particle-particle collisions by $\eta = (1 + e_p)/2$, while the two viscosity factors μ and μ_b , and the thermal conductivity factor λ , are given by

$$\mu = \frac{5M(T/\pi)^{1/2}}{16d^2}; \quad \mu_b = \frac{256\mu\nu^2g_0}{5\pi}; \quad \lambda = \frac{75M(T/\pi)^{1/2}}{8\eta(41 - 33\eta)d^2},$$

where M and d are the mass and diameter of a particle, respectively. For g_0 , which is a function of ν , we choose the form used by Johnson & Jackson (1987), namely

$$g_0(\nu) = \frac{1}{1 - (\nu/\nu_m)^{1/3}},$$

where ν_m denotes the solids volume fraction at closest packing, taken to be 0.65. The values of d , M and the dimensionless factor α used in the present work can be found from table 1.

The granular material does not stick to the wall, so a boundary condition for the slip velocity at the wall must be found by equating the component of the traction on the wall in the direction of slip to the rate of transfer of momentum to the wall by particle impacts. This can be done either in terms of a specific model for the geometry of the wall surface (see, for example, Jenkins & Richman 1986), or in terms of parameters measuring the resiliency of the wall and its effectiveness in scattering incident particles diffusely. With the latter alternative it was shown by Johnson & Jackson (1987) that an appropriate boundary condition for the slip velocity is

$$\mathbf{t} \cdot \boldsymbol{\sigma} \cdot \mathbf{n} + \left(\frac{\pi\sqrt{3}}{6\nu_m}\right)\phi' \rho_p \nu g_0 T^{1/2} \mathbf{u}_{sl} = 0. \quad (8)$$

Here \mathbf{n} is the unit normal to the wall, pointing into the granular material, $\mathbf{u}_{sl} = |\mathbf{u} - \mathbf{u}_w|$ where \mathbf{u}_w is the velocity of the wall and \mathbf{u} that of the granular material in contact with it, and \mathbf{t} is a unit vector tangent to the wall, in the direction of the slip velocity. ϕ' is a 'specularity factor', which measures the fraction of the momentum of an incident particle in the direction of slip which is transmitted, on average, to the wall in a collision. Thus, $\phi' = 1$ for a rough wall which scatters the incident particles with equal probability in all directions, while $\phi' = 0$ for a perfectly smooth wall where scattering is specular.

A boundary condition is also needed for the grain temperature, and this is found by equating the flux of pseudo-thermal energy from the wall to the difference between the rate of generation by slip and the rate of dissipation due to the inelasticity of particle-wall collisions:

$$\mathbf{n} \cdot \mathbf{q} = \left(\frac{\pi\sqrt{3}}{6\nu_m}\right)\phi' \rho_p \nu g_0 T^{1/2} \mathbf{u}_{sl}^2 - \left(\frac{\pi\sqrt{3}}{4\nu_m}\right)(1 - e_w^2) \rho_p \nu g_0 T^{3/2}, \quad (9)$$

where e_w represents the coefficient of restitution for particle-wall collisions.

An increasing number of publications describe a more formal derivation of boundary conditions, based on some specific model of the geometry of the surface of the bounding wall. This approach was pioneered in papers by Jenkins & Richman

Particle diameter, d (m)	0.0018
Solid material density, ρ_p (kg m^{-3})	2980
Particle-particle coefficient of restitution, e_p	0.8
Specularity coefficient for wall collisions, ϕ^p	0.6
Parameter in equation (5), α	1.6

TABLE 1

(1986) and by Richman (1988). When the sizes of the particles and assumed asperities on the wall are both small compared with the macroscopic length scale of the problem, the boundary conditions proposed by these authors reduce to a form essentially the same as that proposed above. There are minor differences in numerical coefficients and in how specifically the form of the functional dependence on ν is specified, but the most significant difference is that the work of Jenkins and Richman relates our specularity factor ϕ^p explicitly to the assumed geometry of the wall. Thus, results obtained with the above boundary conditions and those of Jenkins and Richman should correspond closely, provided the values of the specularity factor in our boundary conditions and the parameter θ (which characterizes the wall geometry) in theirs are mutually consistent.

In addition to studies based on the above boundary conditions, some calculations will also be performed for rather simpler conditions. To motivate these we note that the first term on the right-hand side of (9) represents the rate of generation of pseudo-thermal energy due to slip at the boundary, while the second term represents its rate of dissipation due to the inelasticity of collisions between particles and the boundary. If the value of e_w is close to 1 the former term will dominate, and the boundary will behave as a source of pseudo-thermal energy; if e_w is small, on the other hand, the latter term dominates and the boundary behaves as an energy sink. Both types of boundary will be considered in what follows. The ‘thermal activity’ of the boundary can be suppressed altogether by setting $u_{sl} = 0$ and $e_w = 1$, when both the generation and dissipation terms vanish separately. Solutions can be generated with these two conditions replacing (8) and (9) as boundary conditions. Though they do not represent the conditions at any physically real solid boundary, they nevertheless provide a vital link between the problems of plane shear in layers of bounded and unbounded thickness since, with these conditions, the base state is a velocity field representing uniform shear, while the solids volume fraction and the granular temperature are independent of position, as in the unbounded problem. However, though the base state is now just a slice of finite thickness taken from the corresponding state of the unbounded problem, we shall see that the presence of the bounding walls still has a profound influence on the question of stability. We shall refer to the problem with this type of boundary conditions as the ‘adiabatic case’.

3. Bounded plane shear

Figure 1 shows the configuration to be studied – plane shear between infinite parallel plates – and illustrates some notation. Cartesian coordinates are set up with origin in the central plane, y -axis normal to the planes of shear, and x -axis parallel to the velocity. The upper plate moves to the right and the lower plate to the left, each with speed $u_1/2$, and the plates are separated by a distance Δ . N denotes the normal force per unit area applied to each plate to resist the tendency of the granular material to

$$\begin{aligned}
f_1(\nu) &= \nu[1 + 4\eta\nu g_0(\nu)] \\
f_2(\nu) &= \frac{(2 + \alpha) 5\pi^{1/2}}{288\eta(2 - \eta)} \left(\frac{1}{g_0(\nu)} + \frac{8}{5}\eta\nu \right) [1 + \frac{8}{5}\eta(3\eta - 2)\nu g_0(\nu)] + \frac{8\eta\nu^2 g_0(\nu)(2 + \alpha)}{15\pi^{1/2}} \\
f_3(\nu) &= \frac{25\pi^{1/2}}{16\eta(41 - 33\eta)} \left\{ \left(\frac{1}{g_0(\nu)} + \frac{12}{5}\eta\nu \right) [1 + \frac{12}{5}\eta^2(4\eta - 3)\nu g_0(\nu)] + \frac{64}{25\pi} (41 - 33\eta) \eta^2 \nu^2 g_0(\nu) \right\} \\
f_4(\nu) &= \frac{25\pi^{1/2}}{16\eta(41 - 33\eta)} \left(\frac{1}{\nu g_0(\nu)} + \frac{12}{5}\eta \right) \frac{12}{5}\eta(2\eta - 1)(\eta - 1) \frac{d}{d\nu} [\nu^2 g_0(\nu)] \\
f_5(\nu) &= \frac{48\eta(1 - \eta)\nu^2 g_0(\nu)}{\pi^{1/2}}, \quad f_6(\nu) = \frac{\pi\sqrt{3}\nu g_0(\nu)}{4\nu_m f_3(\nu)} \\
f_7(\nu) &= \frac{\pi\nu g_0(\nu)}{2\sqrt{3}\nu_m f_3(\nu)}, \quad f_8(\nu) = \frac{\pi\nu g_0(\nu)}{2\sqrt{3}\nu_m f_2(\nu)}
\end{aligned}$$

TABLE 2. Dimensionless parameters and functions

force them apart. For steady fully developed flow the y -component of velocity vanishes and, denoting the x -component by u , the above equations of motion reduce to the following form:

$$\frac{d}{dY} \left[f_2 A C T^{*1/2} \frac{du^*}{dY} \right] = 0, \quad (10)$$

$$\frac{D}{DY} [f_1 T^*] = 0, \quad (11)$$

$$\frac{d}{dY} \left[f_3 T^{*1/2} \frac{dT^*}{dY} + f_4 T^{*3/2} \frac{d\nu}{dY} \right] + A^2 f_2 T^{*1/2} \left(\frac{du^*}{dY} \right)^2 - \frac{f_5 T^{*3/2}}{C^2} = 0, \quad (12)$$

where (10) and (11) are the x - and y -components of the momentum balance, respectively, while (12) represents the balance of pseudo-thermal energy. The boundary conditions at the lower plate, $Y = -0.5$, are

$$\frac{du^*}{dY} = \frac{\phi' f_8(u^* + 0.5)}{C}, \quad (13)$$

$$\frac{dT^*}{dY} = -T^* \frac{f_4}{f_3} \frac{d\nu}{dY} + \frac{(1 - e_w^2) f_6 T^*}{C} - \frac{\phi' A^2 f_7 (u^* + 0.5)^2}{C}, \quad (14)$$

and the corresponding conditions at the upper plate are

$$\frac{du^*}{dY} = -\frac{\phi' f_8(u^* - 0.5)}{C}, \quad (15)$$

$$\frac{dT^*}{dY} = -T^* \frac{f_4}{f_3} \frac{d\nu}{dY} - \frac{(1 - e_w^2) f_6 T^*}{C} + \frac{\phi' A^2 f_7 (u^* - 0.5)^2}{C}. \quad (16)$$

Here (13) and (15) come from boundary condition (8), while (14) and (16) represent condition (9); f_1 - f_8 are dimensionless functions of ν , defined in table 2, and dimensionless variables have been introduced, as follows:

$$u^* = u/u_1; \quad T^* = \rho_p T/N; \quad (X, Y) = (x, y)/A. \quad (17)$$

In addition, the equations contain two dimensionless groups, A and C defined by

$$A = \left(\frac{\rho_p u_1^2}{N} \right)^{1/2}; \quad C = \frac{d}{\Delta}, \quad (18)$$

whose physical significance will be discussed below. The total mass M_T of granular material per unit horizontal area is then given by

$$M_T = \rho_p \Delta \int_{-1/2}^{1/2} \nu \, dY \quad (19)$$

so the mean volume fraction of solid material, $\bar{\nu}$, is given by the integral on the right-hand side of (19). Also, the ratio of the magnitudes of the shear and normal stresses is

$$\frac{S}{N} = ACf_2 T^{*1/2} \frac{du^*}{dY}. \quad (20)$$

Before presenting details of the solutions, some of their features can be deduced by inspection. This will also show the significance of the dimensionless groups introduced. Apart from the material properties ϕ' , e_w and e_p (which appears through the factor η in the functions f_1 to f_8), the dimensionless variables ν , u^* and T^* are determined, as functions of X and Y , by the values of the two parameters A and C . In particular, since C determines Δ , the mean volume fraction $\bar{\nu}$ is then determined through (19). Conversely, if $\bar{\nu}$ and Δ are specified, A and C are determined, and hence so are $\nu(X, Y)$, $u^*(X, Y)$ and $T^*(X, Y)$. Then from (18), since A is determined, $N \propto u_1^2$. But (20) shows that the ratio S/N is also determined, so it follows that S too must be proportional to u_1^2 . Finally, (17) shows that $u \propto u_1$ and $T \propto N \propto u_1^2$. All the constants of proportionality in these relations are, of course, determined when $\bar{\nu}$ and Δ/d are specified. Thus A and C may be replaced by $\bar{\nu}$ and Δ/d as equivalent dimensionless parameters, and these have the immediate physical meaning of the mean particle concentration and the dimensionless plate spacing. Note particularly that no additional group specifying the rate of shear, such as a Reynolds number, is needed. The reason for this will become clear, and will be discussed later.

Solutions of the steady-state equations were generated numerically using the finite difference procedure described by Johnson & Jackson (1987), with values for the material properties specified in table 1. Two such solutions are shown in figure 2, each for $\bar{\nu} = 0.35$ and $\Delta/d = 89$, but with different wall conditions. In one case $e_w = 0.97$, and the walls act as sources of pseudo-thermal energy; in a second $e_w = 0.5$, and the walls act as sinks. A third solution is also shown corresponding to the adiabatic case $e_w = 1$, $u_{sl} = 0$, described above. An explicit solution for this case is easily found, namely $\nu = \text{const.} = \bar{\nu}$, $u^* = Y$ and $T^* = A^2 C^2 f_2(\bar{\nu})/f_5(\bar{\nu})$. As noted earlier, it simply represents a slice of thickness Δ taken from an infinite plane shear flow.

The stability of these steady solutions to small perturbations will now be studied. If the motion of the material between the plates is no longer assumed to be steady the boundary conditions (13)–(16) remain unchanged, provided that the plate separation is held constant, but the equations of motion must be replaced by the following set:

$$\frac{\partial \nu}{\partial \tau} + \frac{\partial(\nu u^*)}{\partial X} + \frac{\partial(\nu v^*)}{\partial Y} = 0, \quad (21)$$

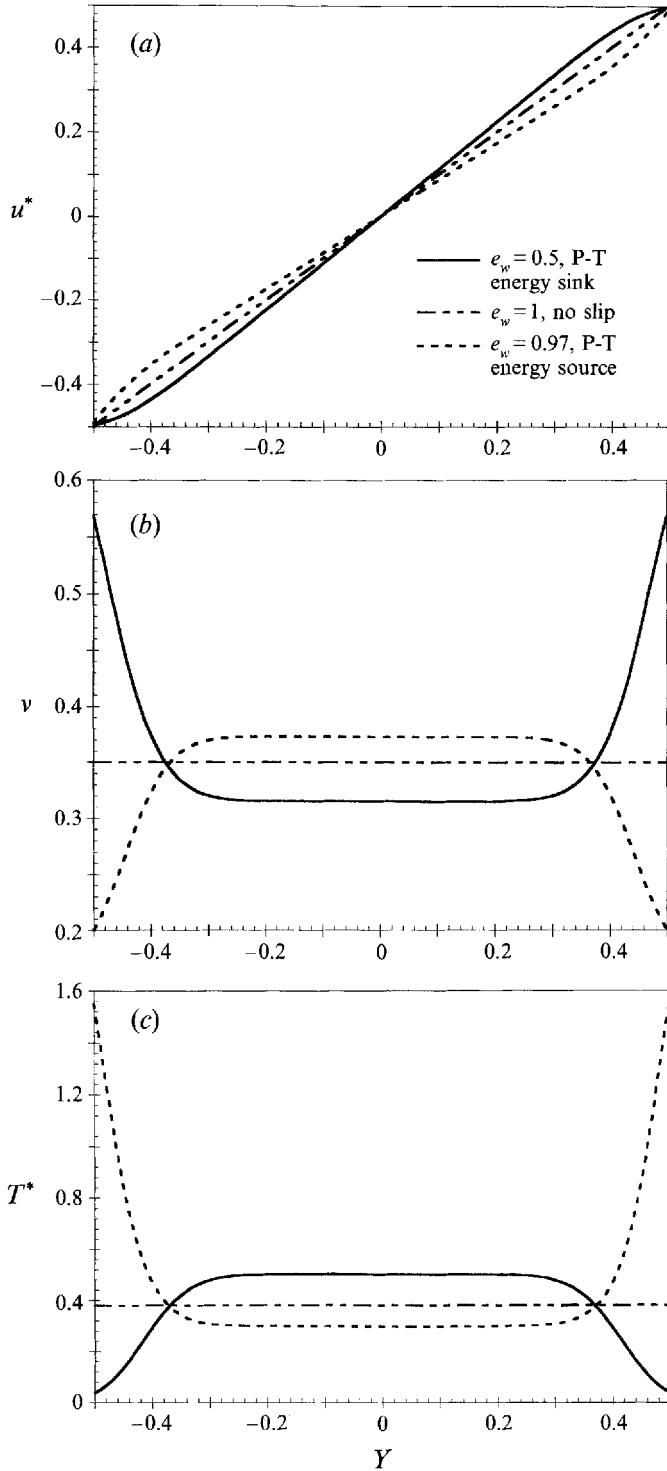


FIGURE 2. (a) Velocity, (b) solids fraction, and (c) grain temperature profiles for steady motion with three different boundary conditions. Parameter values as in table 1, with e_w as indicated on part (a).

$$A^2\nu \left[\frac{\partial u^*}{\partial \tau} + u^* \frac{\partial u^*}{\partial X} + v^* \frac{\partial u^*}{\partial Y} \right] = -\frac{\partial(f_1 T^*)}{\partial X} + \frac{\partial}{\partial Y} \left[f_2 A C T^{*1/2} \left(\frac{\partial u^*}{\partial Y} + \frac{\partial v^*}{\partial X} \right) \right] \\ + \frac{\partial}{\partial X} \left[2f_2 A C T^{*1/2} \left(\frac{2}{3} \frac{\partial u^*}{\partial X} - \frac{1}{3} \frac{\partial v^*}{\partial Y} \right) \right] + \frac{\partial}{\partial X} \left[\frac{8\nu^2}{3\pi^{1/2}} \eta g_0 A C T^{*1/2} \left(\frac{\partial u^*}{\partial X} + \frac{\partial v^*}{\partial Y} \right) \right], \quad (22)$$

$$A^2\nu \left[\frac{\partial v^*}{\partial \tau} + u^* \frac{\partial v^*}{\partial X} + v^* \frac{\partial v^*}{\partial Y} \right] = -\frac{\partial(f_1 T^*)}{\partial Y} + \frac{\partial}{\partial X} \left[f_2 A C T^{*1/2} \left(\frac{\partial u^*}{\partial Y} + \frac{\partial v^*}{\partial X} \right) \right] \\ + \frac{\partial}{\partial Y} \left[2f_2 A C T^{*1/2} \left(\frac{2}{3} \frac{\partial v^*}{\partial Y} - \frac{1}{3} \frac{\partial u^*}{\partial X} \right) \right] + \frac{\partial}{\partial Y} \left[\frac{8\nu^2}{3\pi^{1/2}} \eta g_0 A C T^{*1/2} \left(\frac{\partial u^*}{\partial X} + \frac{\partial v^*}{\partial Y} \right) \right], \quad (23)$$

$$\frac{3A\nu}{2C} \left[\frac{\partial T^*}{\partial \tau} + u^* \frac{\partial T^*}{\partial X} + v^* \frac{\partial T^*}{\partial Y} \right] = \frac{\partial}{\partial X} \left[f_3 T^{*1/2} \frac{\partial T^*}{\partial X} + f_4 T^{*3/2} \frac{\partial \nu}{\partial X} \right] \\ + \frac{\partial}{\partial Y} \left[f_3 T^{*1/2} \frac{\partial T^*}{\partial Y} + f_4 T^{*3/2} \frac{\partial \nu}{\partial Y} \right] - \frac{f_5 T^{*3/2}}{C^2} + \frac{A}{C} \left\{ -f_1 T^* \left(\frac{\partial u^*}{\partial X} + \frac{\partial v^*}{\partial Y} \right) \right. \\ \left. + f_2 A C T^{*1/2} \left[\left(\frac{\partial u^*}{\partial Y} + \frac{\partial v^*}{\partial X} \right)^2 + \frac{4}{3} \left(\left(\frac{\partial u^*}{\partial X} \right)^2 - \left(\frac{\partial u^*}{\partial X} \right) \left(\frac{\partial v^*}{\partial Y} \right) + \left(\frac{\partial v^*}{\partial Y} \right)^2 \right) \right] \right\} \\ + \frac{8\nu^2}{3\pi^{1/2}} \eta g_0 A^2 T^{*1/2} \left(\frac{\partial u^*}{\partial X} + \frac{\partial v^*}{\partial Y} \right)^2. \quad (24)$$

Equation (21) is the continuity equation, which is satisfied trivially by the steady-state solution, (22) and (23) are the two components of the momentum equation, and (24) represents the balance of pseudo-thermal energy. The y -component of velocity now no longer vanishes, and its dimensionless value is denoted by v^* , while a dimensionless time τ is defined by $\tau = tu_1/\Delta$.

These equations are then linearized in the usual way for small perturbations about the steady-state solution. Distinguishing the steady state by suffix zero, we explore perturbations of the following form:

$$\left. \begin{aligned} u^* &= u_0(Y) + u' \quad \text{where} \quad u' = u_e(Y) \exp(\Omega\tau) \exp(iK_x X), \\ v^* &= v' = v_e(Y) \exp(\Omega\tau) \exp(iK_x X), \\ \nu &= \nu_0(Y) + \nu' \quad \text{where} \quad \nu' = \nu_e(Y) \exp(\Omega\tau) \exp(iK_x X), \\ T^* &= T_0(Y) + T' \quad \text{where} \quad T' = T_e(Y) \exp(\Omega\tau) \exp(iK_x X). \end{aligned} \right\} \quad (25)$$

The result of these substitutions and the subsequent linearization is a set of simultaneous ordinary differential equations for u_e , v_e , ν_e and T_e , as functions of Y , with coefficients which depend on the base-state solution and are in principle, therefore, known functions of Y . The equations of motion and the process of linearization are, of course, the same as those used in the studies of the unbounded problem referred to above, though extra terms arise because the base states are, in general, no longer spatially uniform. However, the imposition of the boundary conditions (13)–(16) constrains the perturbation modes to the form (25). The boundary conditions can similarly be translated into boundary conditions on u_e , v_e , ν_e and T_e , and when these are joined with the above differential equations an eigenvalue problem for Ω results. The coefficients in the differential equations and boundary conditions depend on the particular base-state solution and its spatial derivatives, and to speed up their calculation an interpolator representing the base state in an explicit algebraic form is needed. Because of the form of typical base states (see figure 2), except for the adiabatic

case no single polynomial provides an adequate fit over the whole width of the shear layer, and a piecewise polynomial approximation was therefore used.

The eigenvalue problem for the differential equations satisfied by the modal variables is finally translated into a matrix eigenvalue problem by discretizing the equations using a finite difference approximation. Typically the interval $[-0.5, 0.5]$ for Y is divided into 100 equal sub-intervals, and u_e, v_e and T_e are evaluated at the 101 grid points (including the two boundaries). The volume fraction v_e , on the other hand, is evaluated at the mid-points of the sub-intervals, resulting in one less unknown for this variable in the matrix formulation. Explicitly detailed form of the above equations are too cumbersome to be reproduced here, but can be found in Wang (1995).

The eigenvalues are computed using the software *Mathematica*, for a sequence of values of the wavenumber K_x . In what follows the eigenvalue with the largest real part, for a given value of K_x , will be referred to as the *leading eigenvalue* for that value of K_x . Among the leading eigenvalues, for all values of K_x , the one with the largest value of Ω_r will then be referred to as the *dominant eigenvalue*. This identifies a dominant eigenvalue for each point in the $(\bar{v}, \Delta/d)$ -plane, and the sign of its real part determines the linear stability of the corresponding steady state.

It is important to note that the full equations (21)–(24), describing unsteady motion, introduce no new dimensionless parameters in addition to A and C . Thus, the values of all the dimensionless variables for general unsteady solutions are also determined by specifying values for these two parameters or, equivalently, specifying the values of \bar{v} and Δ/d . In particular, the dimensionless growth rate Ω_r is determined, so the corresponding dimensional growth rate $\omega_r (= \Omega_r u_1/\Delta)$ is proportional to the shear rate, with the factor of proportionality determined by the values of \bar{v} and Δ/d . It also follows that the condition of neutral stability, $\Omega_r = 0$, establishes a relation between \bar{v} and Δ/d : in other words there is a neutral stability curve in the $(\bar{v}, \Delta/d)$ -plane, and this is unaffected by the value of the rate of shear. The amount of growth of any perturbed variable a between t_1 and t_2 , measured by $\ln(a_2/a_1)$, is proportional to the amount of shear, $u_1(t_2 - t_1)/\Delta$.

These features are counterintuitive to one familiar with stability problems of Newtonian fluids. Among other things they imply that no Reynolds number has a significant role in determining stability. Indeed, since the steady states in general have non-uniform particle concentration and grain temperature, both the bulk density and the effective viscosity vary widely over the region between the plates, and there is no unique way of defining a Reynolds number. For the adiabatic case alone these quantities are constant over the width of the layer in the steady state, and a unique Reynolds number can then be defined for each base state. However, the viscosity which appears in its denominator is proportional to $T^{1/2}$ which is found, in turn, to be proportional to the rate of shear. Consequently the value of the Reynolds number is independent of the shear rate and, unlike the case of a Newtonian fluid, it does not provide a dimensionless measure of the velocity. This is the underlying reason for the conspicuous absence of the Reynolds number from most work on granular materials. Despite its lack of relevance there is no difficulty in calculating a Reynolds number for the adiabatic case, based on the layer thickness and the plate speed, and for the solution illustrated in figure 2, where $\bar{v} = 0.35$ and $\Delta/d = 89$, its value is 2310.

4. Results for the bounded shear layer

Figure 3 shows a stability diagram in the plane of \bar{v} and d/Δ , determined as just described, for the case $e_w = 0.5$, when the walls act as energy sinks, and with other

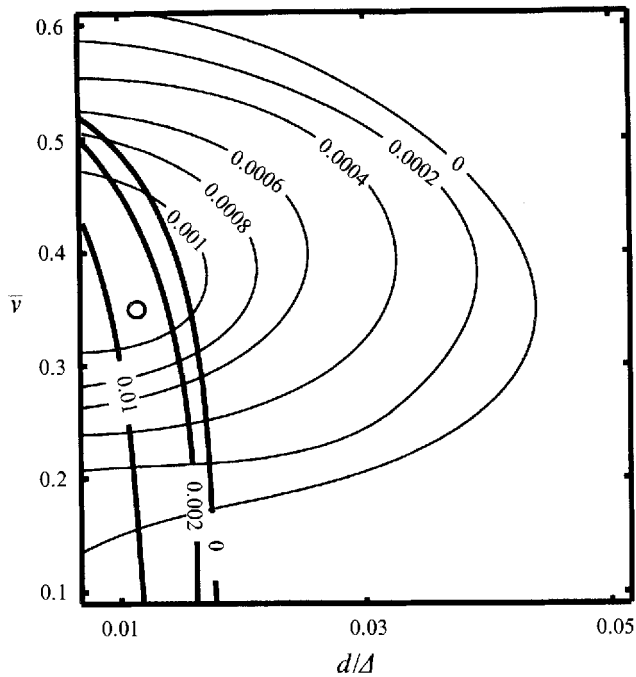


FIGURE 3. Contour map of the dimensionless instability growth rate, Ω_r , in the $(\bar{v}, d/\Delta)$ -plane. Parameter values as in table 1, with $e_w = 0.5$ (energy sink at walls). Light curves correspond to the layering mode, heavy curves to the stationary mode.

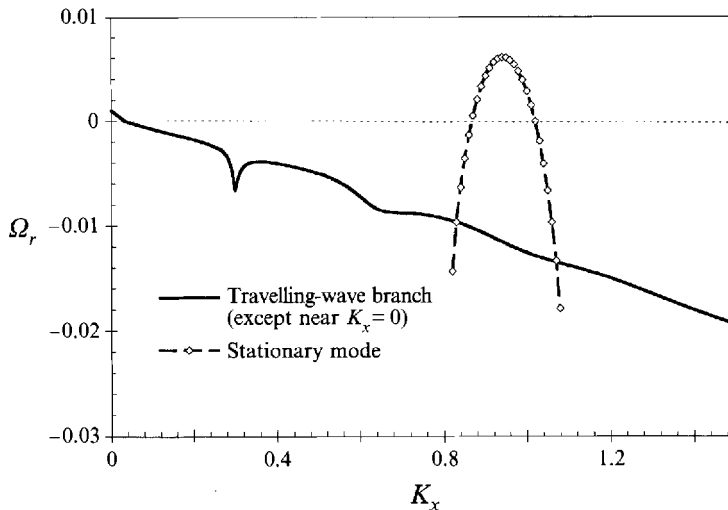


FIGURE 4. Growth rate versus wavenumber K_x , for the least-stable travelling wave modes and for the dominant stationary mode, at the point $(\bar{v}, \Delta/d) = (0.35, 89)$. Parameter values as for figure 3.

parameter values as listed in table 1. Some contours of constant growth rate for the dominant eigenvalue are shown in the unstable region, labelled with the corresponding values of Ω_r ; the limiting stability boundary is then the contour labelled zero. It is seen that the system is always stabilized at sufficiently large values of d/Δ , that is, when the plates are brought sufficiently close together. The range of instability is largest when

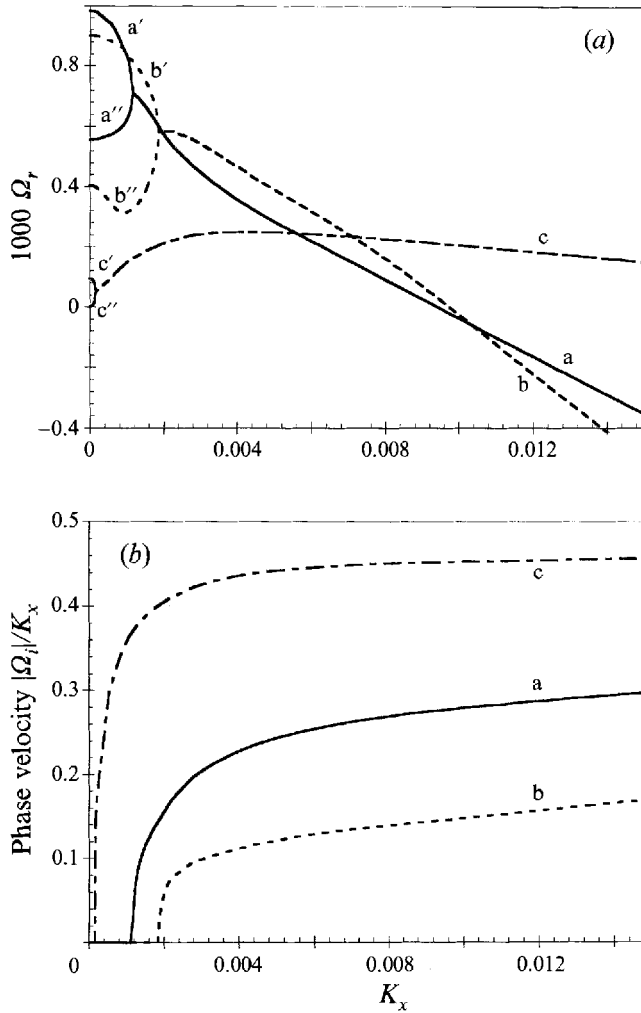


FIGURE 5. (a) Growth rates for the least-stable modes at very small values of K_x . (b) Magnitude of the phase velocity for each of the modes shown in (a). Parameter values as for figure 3. $(\bar{\nu}, \Delta/d) = (0.35, 89)$.

$\bar{\nu} \approx 0.35$, falling off quite quickly on both sides of this value. Within the region of instability two sets of contours of Ω_r are shown, distinguished by light and heavy lines. The larger part of the stability boundary is formed by the null contour of the first set but, at a value of $\bar{\nu}$ between 0.1 and 0.2, this is crossed by the null contour of the second set, which then becomes the stability boundary for smaller values of $\bar{\nu}$. Evidently the two sets of contours represent dominant eigenvalues belonging to different branches. The growth rates for the first set are quite small, while those for the second set rapidly increase to much larger values on moving to the left from the null contour of that set. If Ω_r is regarded as a third dimension of the diagram, the eigenvalues of the first set form a gently rising hill, starting from 'sea level' at the null contour, while those of the second set form a steep escarpment which pushes up through this hill.

We will now trace in detail the relation between these two sets of eigenvalues and examine the nature of the corresponding eigenfunctions. For this purpose we select one point of figure 3, namely $(\bar{\nu}, \Delta/d) = (0.35, 89)$, which lies to the left of the null contour

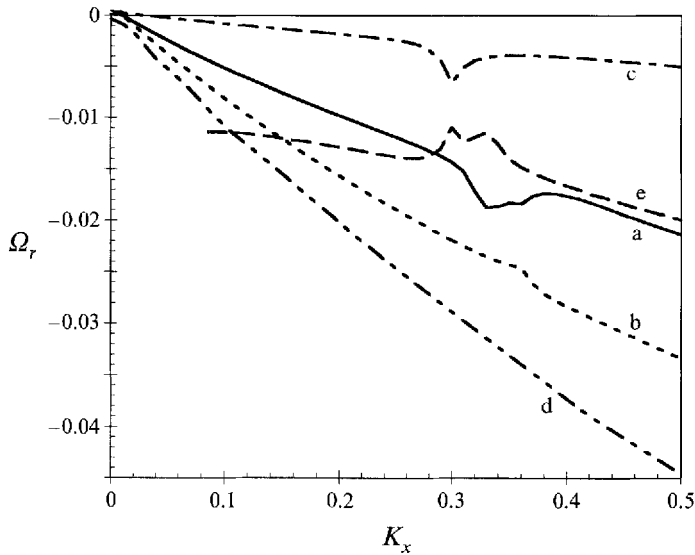


FIGURE 6. Growth rates for the five least-stable modes in the interval $0 < K_x < 0.5$, illustrating the crossing of branches. Parameter values as for figure 3. $(\bar{v}, \Delta/d) = (0.35, 89)$.

for the second set; its position is indicated by an open circle in figure 3. Then figure 4 shows the real part of the leading eigenvalue, as a function of K_x , and it is apparent that at least two branches of eigenvalues are represented. For very small values of K_x the value of Ω_r is positive, indicating instability, but a much stronger instability is associated with eigenvalues from another branch, for which Ω_r assumes its largest value near $K_x = 0.95$. This then identifies the dominant eigenvalue when $(\bar{v}, \Delta/d) = (0.35, 89)$.

To understand what is happening in figure 4 the interval of K_x shown must be split into sub-intervals and several of the branches of eigenvalues with the largest values of Ω_r must be shown so that their relationship can be traced. Figure 5(a) shows a magnified view of the three branches of eigenvalues with the largest growth rates over a very short interval of K_x adjacent to $K_x = 0$. When $K_x > 0.002$ the three distinct branches, labelled a, b and c, respectively, represent harmonic waves of the form (25), which travel in the x -direction with phase velocity $-\Omega_i/K_x$ and have wavefronts which are modulated in the y -direction. Each point on one of the above branches represents a pair of waves of this sort, propagating in the positive and negative x -directions, respectively, but otherwise identical. (This merely reflects the antisymmetry of the steady-state velocity field about the central plane; the two solutions are physically the same wave.) Their phase velocities are shown in figure 5(b) and for each branch it is seen that the velocity vanishes in some interval of K_x adjacent to $K_x = 0$. Within this interval figure 5(a) shows that each branch splits into two parts, labelled a', a'' etc., and the eigenfunctions now represent stationary patterns of density and velocity variations, harmonic in the X -direction, whose amplitudes grow or decay exponentially depending on the sign of Ω_r . We shall refer to eigenfunctions of this type as *stationary modes*, in contrast with the *travelling wave modes* found for larger values of K_x . (It should be noted that behaviour of the type just described is not peculiar to granular materials: a similar branching pattern was reported by Gallagher & Mercer (1962) who studied the stability of a plane shearing layer of a Newtonian fluid though, in that case, all the eigenvalues had negative real parts.)

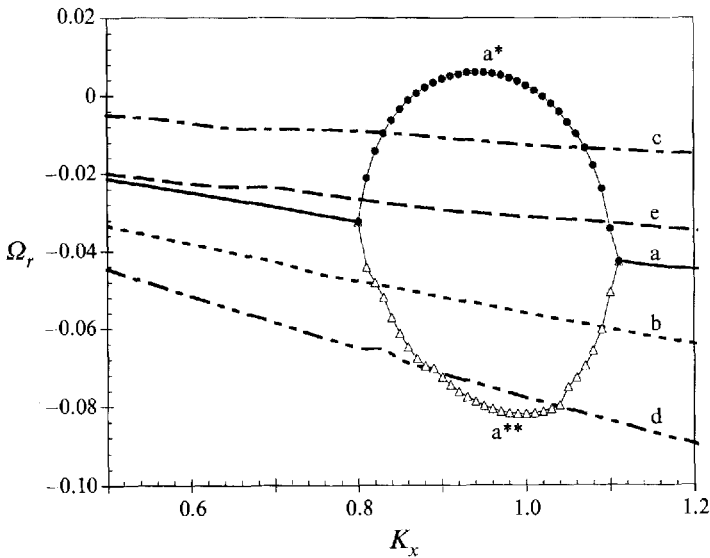


FIGURE 7. Growth rates of the five least-stable modes in the interval $0.5 < K_x < 1.2$, illustrating the origin of the branch a^* of stationary modes which contains the dominant eigenvalue. Parameter values as for figure 3. $(\bar{\nu}, A/d) = (0.35, 89)$.

Note that the branches shown in figure 5(a) cross each other in a rather complicated way so that the leading eigenvalue switches from branch to branch. When $K_x = 0$ the leading eigenvalue belongs to branch a' and it is unstable. At $K_x \approx 0.001$ the a' and b' branches cross, so branch b' becomes the leading eigenvalue. Further crossings then shift the leading eigenvalue successively to branches b and c as K_x increases. The picture is extended to a larger interval of K_x in figure 6 where two more branches, labelled d and e , are added. The leading eigenvalue remains on the branch c throughout this interval, and it represents a travelling wave mode. However, except for a short interval adjacent to $K_x = 0$ the real part of this eigenvalue is negative. Branch e , which is not one of the least-stable branches at $K_x = 0$, crosses all but branch c and therefore represents the second mode when $K_x > 0.29$.

The interval $0.5 < K_x < 1.2$ is shown in figure 7, with each of the branches from figure 6 continued. As K_x increases from 0.5 the leading eigenvalue initially belongs to branch c , while the eigenvalues of branch a lie in third position. However, at $K_x \approx 0.8$ the phase velocity of the waves from branch a falls to zero, and this branch splits into a new pair of branches, identified as a^* and a^{**} , which represent stationary modes. Branches a^* and a^{**} recombine at $K_x \approx 1.12$, beyond which branch a continues and represents travelling wave modes once more. The largest value of Ω_r on branch a^* , which is attained at $K_x = 0.95$, is positive and is substantially larger than any other value of Ω_r encountered for $K_x \leq 1.2$. We can now see that the prominent second branch represented on figure 4 is just this branch a^* .

A value $K_x = 1.2$ represents a wavelength of approximately 470 particle diameters, so substantially larger values of K_x remain physically significant. The eigenvalue computations were, therefore, extended to $K_x = 600$, when the wavelength is comparable with the particle diameter. Beyond $K_x = 1.2$ the leading eigenvalue was found to switch branches three more times, but it continued to representing travelling wave modes throughout, and its real part never again became positive. Thus, the peak of branch a^* , at $K_x = 0.95$, gives the dominant eigenvalue for this point in the $(\bar{\nu}, A/d)$ -

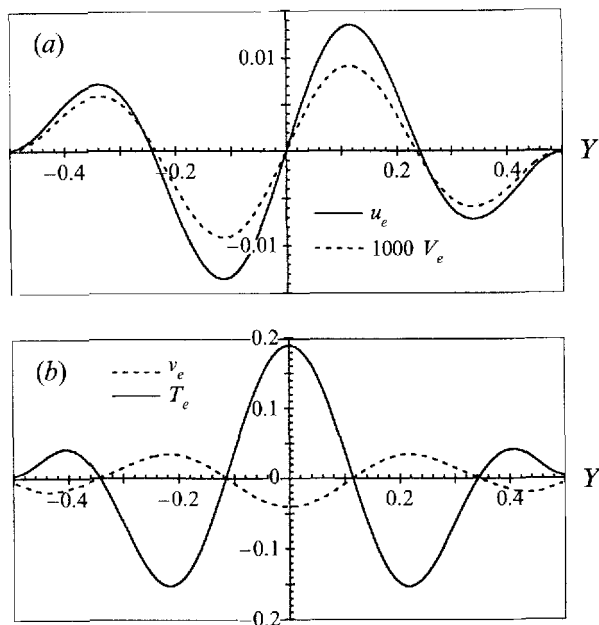


FIGURE 8. Eigenfunctions of the fastest growing layering mode ($K_x = 0$). (a) u_e and v_e , (b) v_e and T_e . Parameter values as for figure 3. $(\bar{v}, \Delta/d) = (0.35, 89)$.

plane. (We did not investigate whether more structures like that of branches a* and a** in figure 7 occur anywhere in this extended interval of K_x but, if they do, they never contain the leading eigenvalue.) The mode with the second largest growth rate for these values of $(\bar{v}, \Delta/d)$ is again a stationary mode, corresponding to branch a' at $K_x = 0$. For this mode there is no structure in the x -direction and the particles form plane layers of alternating higher and lower concentration, parallel to the planes of shear. Stationary modes of this type will be called *layering modes*. They are of interest because, as we shall see, they are related to the unstable modes of an unbounded shear flow.

On decreasing the value of Δ the representative point moves to the right in figure 3 and, correspondingly, the height of the peak of branch a* subsides until it is less than that of branch a' (figure 5a) at $K_x = 0$. The latter then takes over as the dominant eigenvalue, and in figure 3 the escarpment represented by the heavy contours drops below the hill represented by the light contours.

We turn now to the nature of the eigenfunctions. For the layering modes ($K_x = 0$) these can be represented fully by plotting u_e, v_e, v_e and T_e as functions of Y , and this is done in figure 8. It is seen that u_e and v_e are odd functions of Y , with v_e much smaller than u_e , while v_e and T_e are even functions. The grain temperature is largest at $Y = 0$ and the two profiles oscillate out of phase, with the particle concentration high where the temperature is low.

Stationary modes are found for small values of K_x on branch a', and also for larger values of K_x on branch a*. Figure 9 shows the particle volume fraction distribution corresponding to the stationary-mode eigenfunction from branch a', figure 5(a), at $K_x = 0.0002$. It is represented on a grey scale, with black corresponding to high density and contours drawn at equal increments of the volume fraction. There are seen to be alternating bands of higher and lower density, inclined roughly equally to the two axes, and within each band there is a row of five compact regions of increased, or decreased

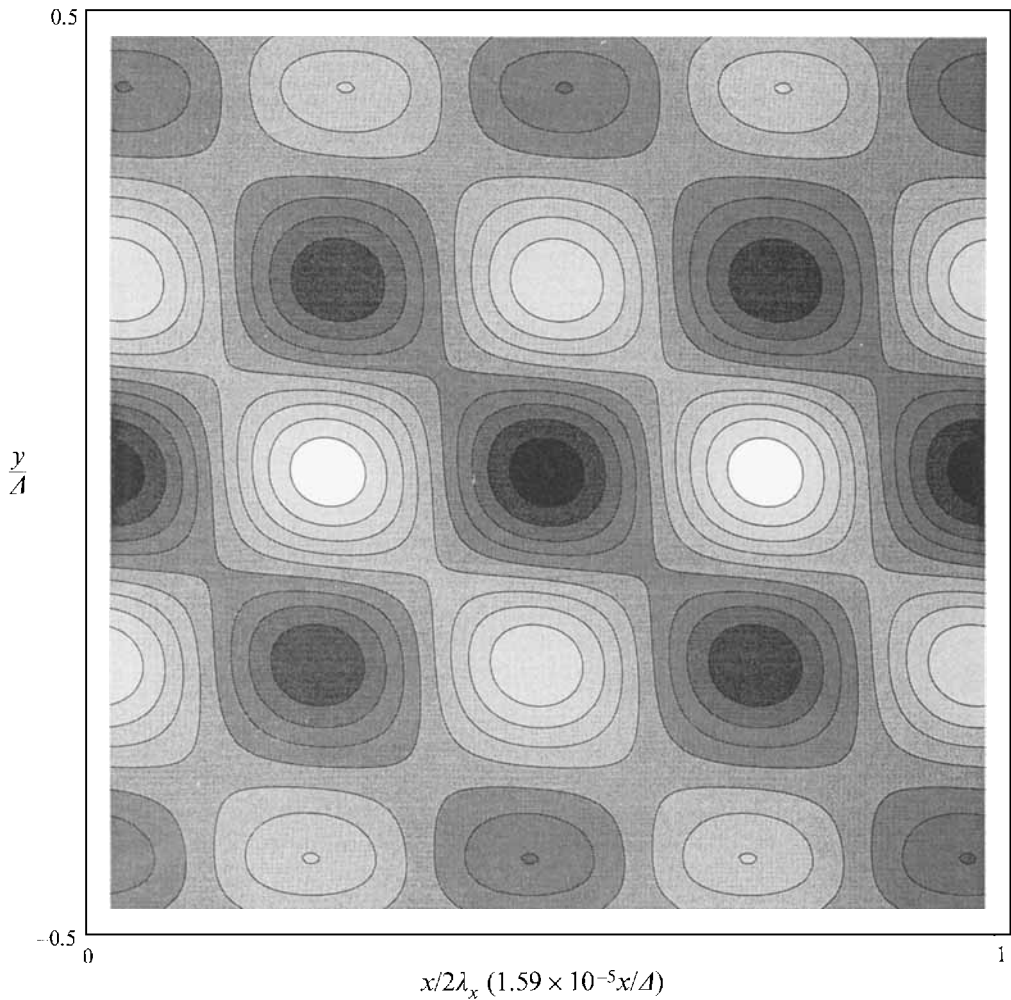


FIGURE 9. Stationary-mode eigenfunction $v(x, y)$ (i.e. $\text{Re}[v_e(Y)\exp(iK_x X)]$) at a point on the stationary mode branch a' , with $K_x = 0.0002$. Parameter values as for figure 3. $(\bar{v}, A/d) = (0.35, 89)$.

density. However, this description is somewhat misleading as the abscissa has been scaled on twice the (very large) wavelength in the x -direction. This compression of distance in the direction of shear is necessary for reasonably compact presentation, but the reader should understand that the picture must be stretched enormously in the x -direction to give a true sense of the inclination of the bands, which are quite near to the limit where they degenerate into layers parallel to the shear planes. The factor by which the abscissa must be changed to match the scale of the ordinate is shown explicitly on the diagram.

The volume fraction distribution of the dominant stationary mode, belonging to branch a^* at $K_x = 0.95$, is shown in figure 10, using the same form of representation as in figure 9. There are, once again, alternating bands of high and low density inclined to match the direction of shear, but now within each band there are only three compact regions of increased or decreased density, with the two most pronounced occurring almost in contact with the bounding plates, while the third, which is much weaker, is located on the central plane. Again the picture is compressed in the x -direction, as

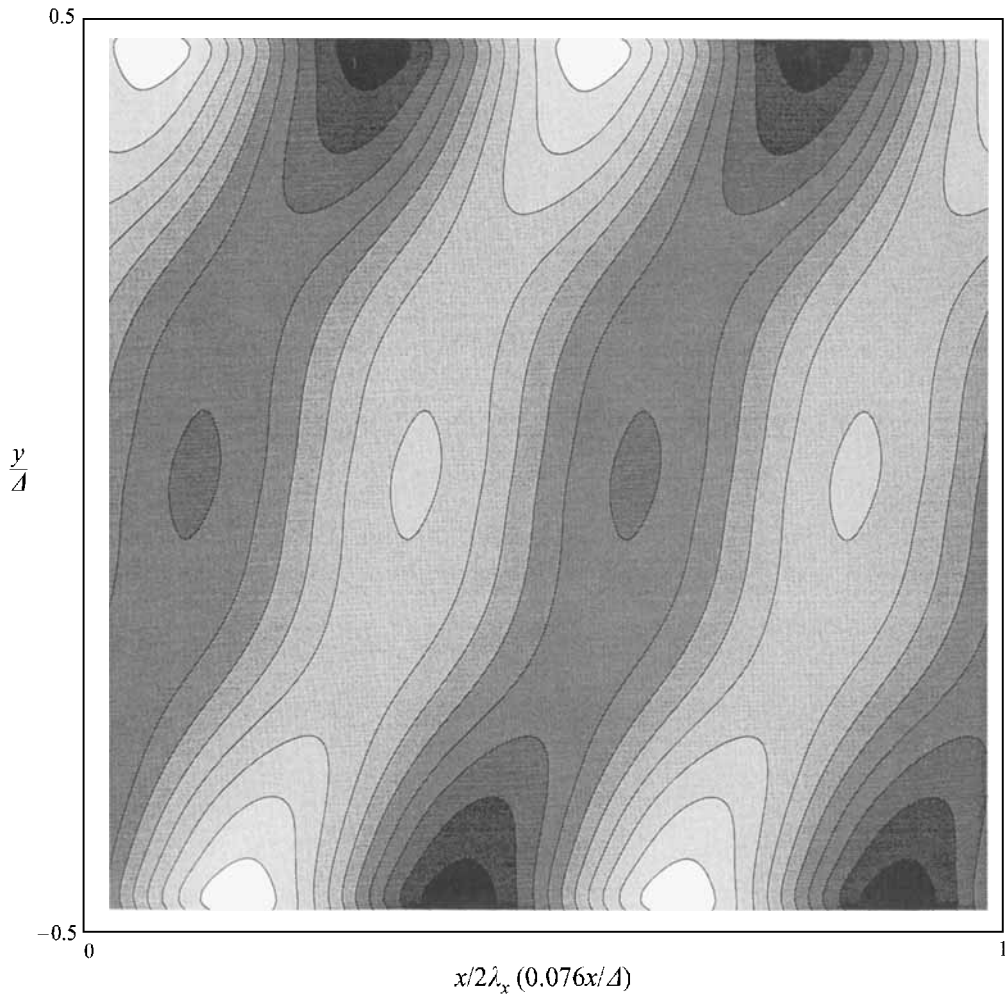


FIGURE 10. Dominant stationary-mode eigenfunction $v(x, y)$ at $K_x = 0.95$. Parameter values as for figure 3. $(\bar{v}, \Delta/d) = (0.35, 89)$.

indicated, but much less so than figure 9. A realistic picture of the distribution of particle concentration is obtained by stretching the diagram about thirteen times in this direction. In both figures 9 and 10 it must be emphasized that the inclination of the bands is independent of the magnitude of the overall shear rate, though a reversal of the directions of motion of the plates would reverse the inclination.

Though the stationary modes described above contain regions of enhanced particle concentration these do not resemble the clusters which have been observed in dynamic simulations, since they do not convect with the mean motion of the material but form a pattern that remains at rest in the frame of the central plane of the shearing layer. Structures analogous to the convected clusters are, however, seen in the leading travelling wave modes. Thus, figure 11 shows an instantaneous density distribution for the leading mode at $K_x = 0.7$. Reference to figure 7 shows that this is a travelling wave, and its dimensionless phase velocity is 0.486. The distribution shown in figure 11 corresponds to the wave travelling to the right with this velocity; rotation of the figure by 180° gives the density distribution for the second eigenfunction, which is a wave moving to the left with the same speed. The most prominent feature of figure 11 is a

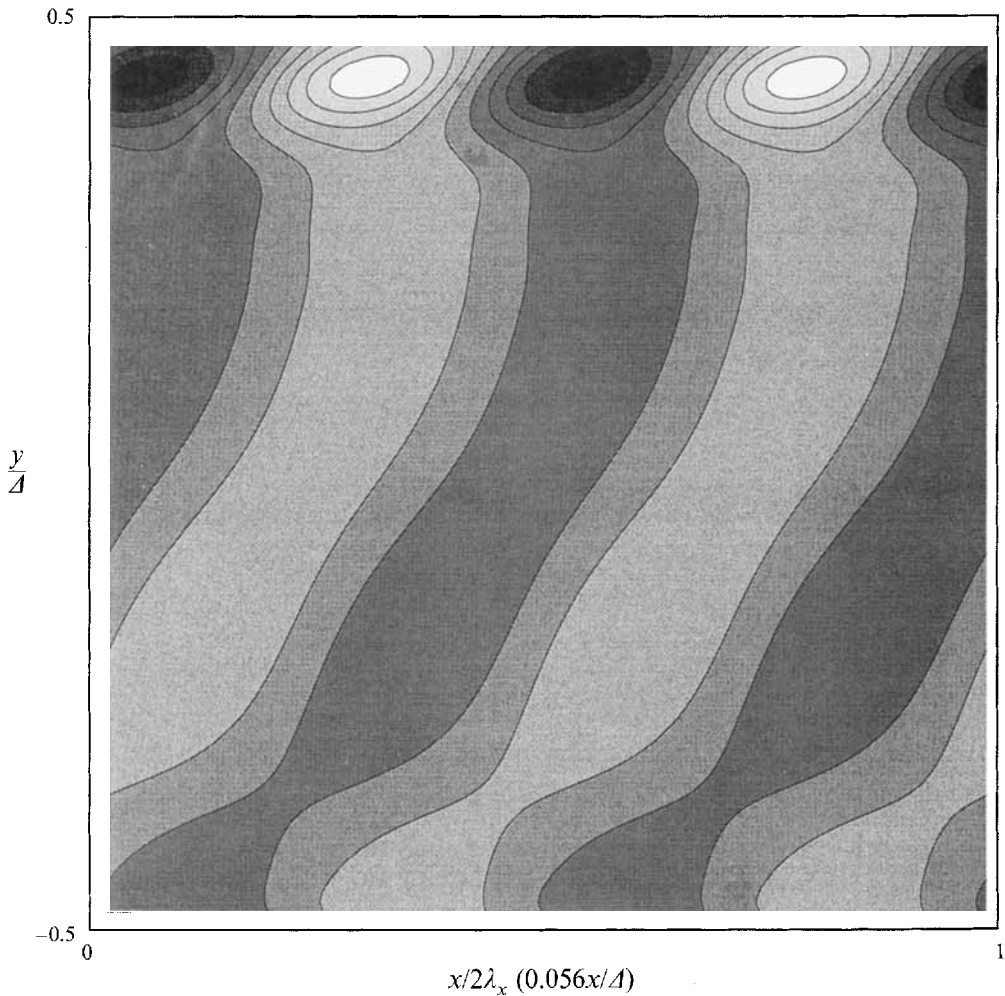


FIGURE 11. Leading travelling-wave eigenfunction $v(x, y)$ at $K_x = 0.7$. Phase velocity = 0.486. $(\bar{v}, A/d) = (0.35, 89)$. Parameter values as for figure 3.

row of clusters quite close to the upper bounding plate, and it is easy to check that the mean velocity of the base solution, at the position of their centres, matches closely the value of the phase velocity of the wave, quoted above. Thus, these clusters convect with the mean motion of the material. If the waves propagating in the opposite direction are superimposed a solution is obtained which consists of a row of clusters near each wall, propagating to the left and right, respectively, each with the mean velocity of the material in its neighbourhood. The region between them is occupied by a complicated, periodically varying concentration pattern. However, the analogy with the clusters seen in simulations should not be pressed too far. In order to see a faithful representation of the appearance of the density pattern the scale of the abscissa in figure 11 should be stretched about eighteen times, so the 'clusters' seen there are by no means as compact as they appear to be. Furthermore, though they belong to the leading mode at $K_x = 0.7$, the growth rate of this mode is negative, so they would not be expected to appear spontaneously. Indeed, the leading mode is an unstable travelling wave only for very small values of K_x (see figure 5a), so any convecting 'clusters' which might form spontaneously would be elongated enormously in the direction of shear.

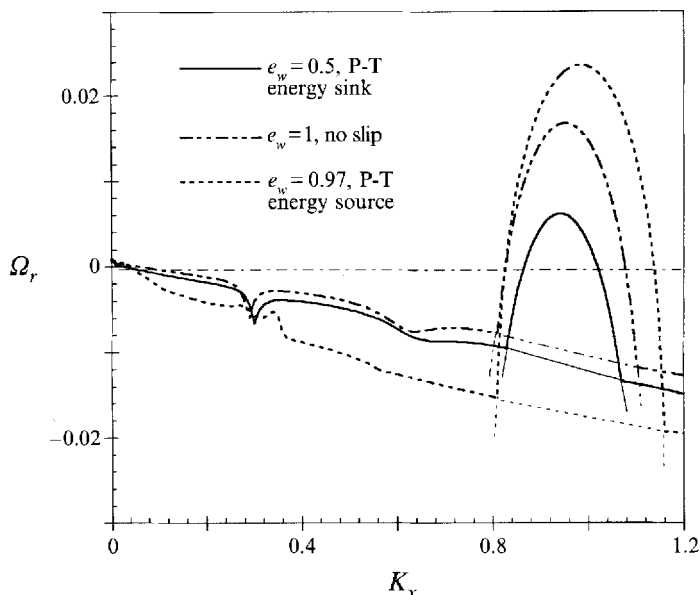


FIGURE 12. Growth rate versus wavenumber, K_x , for the leading modes at the point $(\bar{\nu}, \Delta/d) = (0.35, 89)$. Parameter values as in table 1. Results shown for three different values of e_w to illustrate the effect of changing the boundary conditions.

So far the discussion has been limited to one point in the parameter space, $(\bar{\nu}, \Delta/d) = (0.35, 89)$, and to one particular boundary condition, $e_w = 0.5$, where the walls act as sinks for the pseudo-thermal energy. We now examine the effect of changing the boundary condition. Figure 12 is analogous to figure 4 but, in addition to the results for $e_w = 0.5$ (which are simply a copy of figure 4), corresponding results are shown for the adiabatic case ($e_w = 1, u_{sl} = 0$) and for a case with $e_w = 0.97$, when the walls act as sources of pseudo-thermal energy. In each case the general picture is the same. The dominant eigenvalue is at the peak of a stationary-mode branch, and the position of this peak changes only between $K_x \approx 0.95$ and $K_x \approx 1.0$ as the boundary condition is changed. However, the height of the peak increases from $\Omega_r \approx 0.006$ to $\Omega_r \approx 0.024$ on changing from the energy sink boundary condition, through the adiabatic case, to the energy source condition. The eigenfunctions for the dominant mode change very little when the boundary conditions are altered. The distribution of ν for the dominant eigenfunction with the energy-sink boundary condition has already been shown in figure 10; the corresponding results for the adiabatic case and for the energy-source boundary condition are shown in figures 13 and 14, respectively. There is seen to be very little difference between the three cases. The only perceptible change is a slight movement of the most prominent regions of high and low density away from the walls on progressing from the sink case, through the adiabatic case, to the source case.

Turning to the effect of shifting the point in the $(\bar{\nu}, \Delta/d)$ -plane, we have already pointed out that the dominant peak in figure 4 shrinks in height when Δ is decreased, eventually leaving the point on the highest branch at $K_x = 0$ as the dominant eigenvalue, with a switch from a stationary mode, with structure in the x -direction, to layering as the dominant mode. To investigate the effect of varying Δ/d over a wide range of values it is easiest to focus on the ‘adiabatic’ boundary conditions corresponding to $e_w = 1, u_{sl} = 0$, since then the density is uniform and the velocity

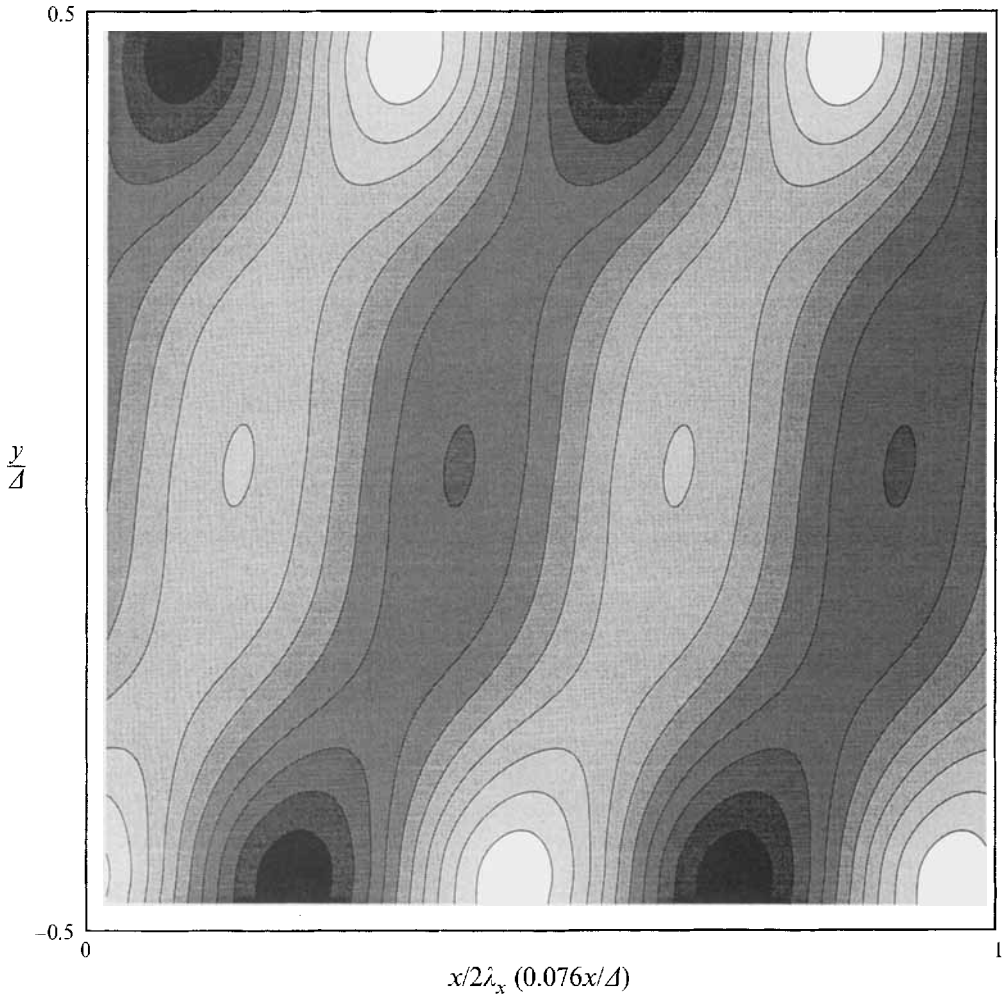


FIGURE 13. Dominant stationary-mode eigenfunction $v(x, y)$ at $K_x = 0.95$. $(\bar{\nu}, A/d) = (0.35, 89)$. Parameter values as for figure 10, except that wall boundary conditions are changed to $e_w = 1, u_w = 0$, the adiabatic case.

varies linearly within the sheared layer in the base state. This saves the time needed to construct adequately accurate piecewise polynomial representations of the base states for large plate separations. Then, with $\bar{\nu}$ fixed at 0.35, figure 15 shows the maximum value of Ω_r and the corresponding wavenumber K_x , as functions of A/d . The transition from the stationary mode with $K_x \neq 0$ to layering, with $K_x = 0$, as the dominant mode occurs at a value of A/d between 50 and 60, and it is marked by a discontinuous drop in the value of K_x . For larger values of A/d the dominant eigenvalue belongs to a stationary mode and, as A/d increases, Ω_r passes through a maximum near $A/d = 100$ then falls again for as long as the computations were continued. At the same time K_x decreases monotonically and appears to be tending to zero as A/d increases without bound.

The eigenfunctions of the density distribution, for the four conditions labelled a, b, c and d in figure 15, are shown in the correspondingly labelled panels of figure 16 where, as before, the ordinate and abscissa are y/D and $x/2\lambda_x$, respectively. When plotted in

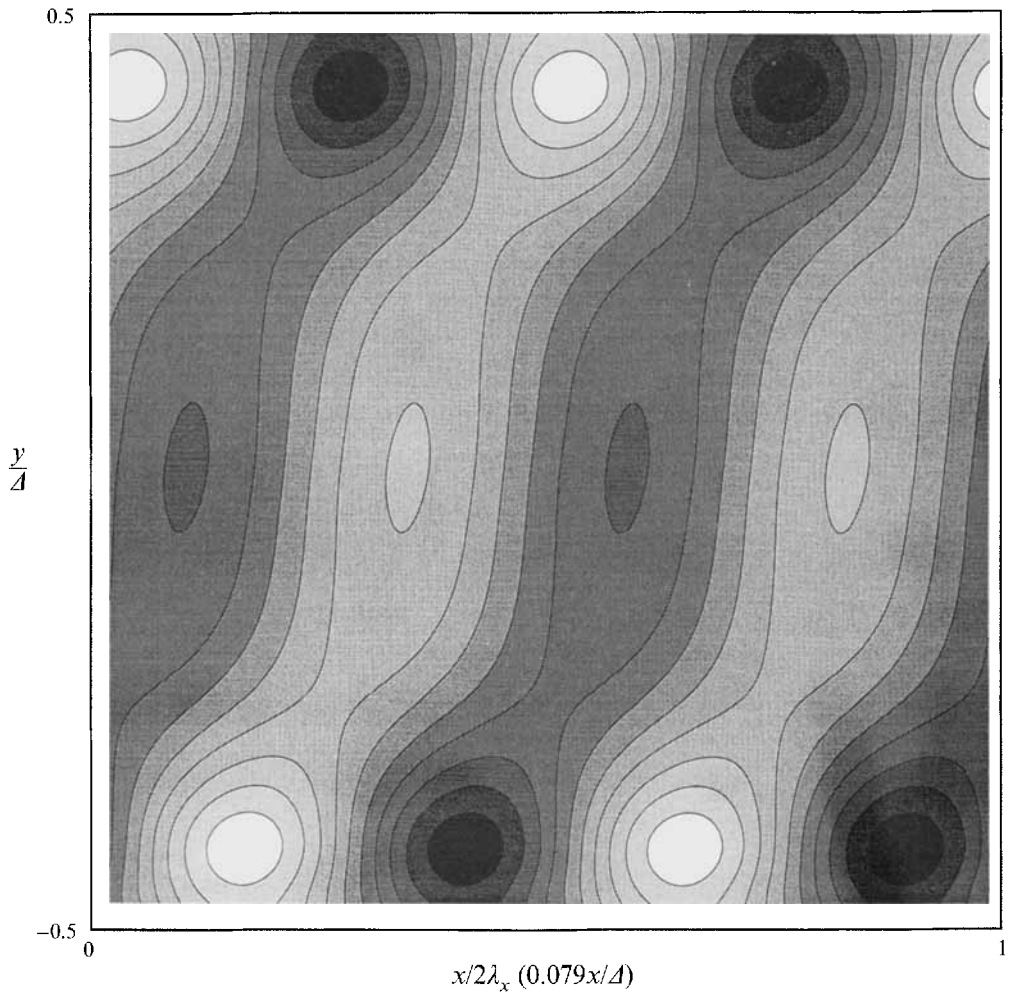


FIGURE 14. Dominant stationary mode eigenfunction $v(x, y)$ at $K_x = 1.0$. $(\bar{v}, \Delta/d) = (0.35, 89)$. Parameter values as for figure 10, except that the value of e_w is changed to 0.97, corresponding to an energy source at the walls.

this way there are only minor changes in the eigenfunction as Δ/d varies, but of course the true orientation of the inclined bands of higher and lower density is seen only if the abscissa is replaced by x/Δ . For each panel of figure 16 the scale factors relating x/Δ to $x/2\lambda_x$ are therefore given in the caption, and it is seen that the pattern of bands actually rotates toward a horizontal orientation as Δ/d increases. At the same time the rate of growth of the instability decreases, so the dominant stationary mode approaches a weak layering type of instability at large values of Δ/d . In summary, then, the stationary mode with structure in the x -direction is not dominant at small plate separations, but its rate of growth increases as the plates are moved apart, and it soon dominates the layering instability. With further increase in plate separation the rate of growth passes through a maximum, then decreases. At the same time the orientation of the bands of higher and lower density rotates toward the horizontal, and there is an indication that the stationary mode may degenerate asymptotically into a layering mode as the plate separation increases without bound.

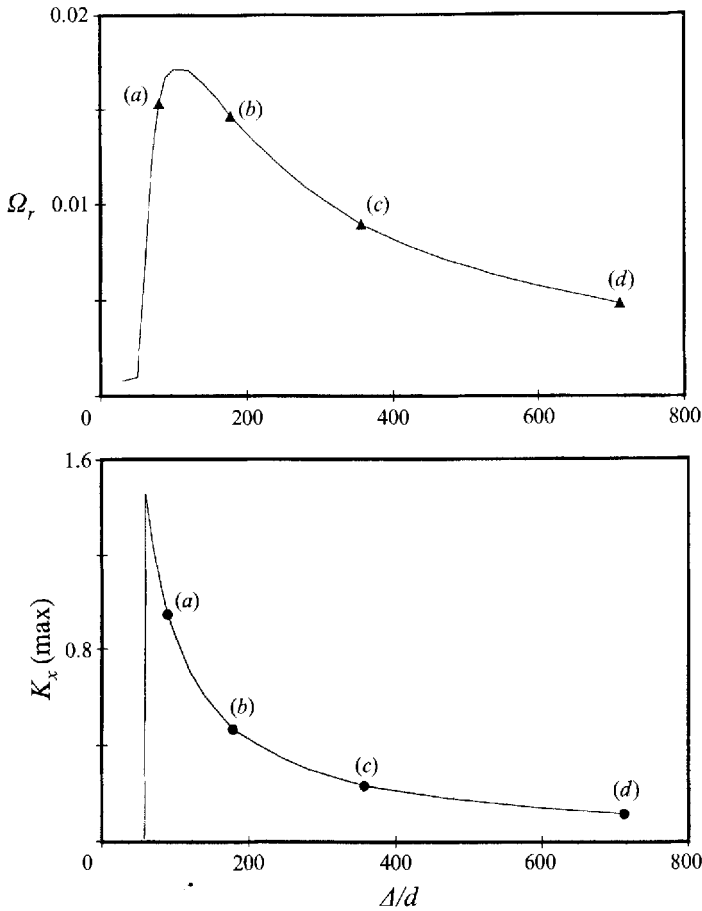


FIGURE 15. Dependence of growth rate and wavenumber on plate separation for the dominant mode, with $\bar{\nu} = 0.35$ and the boundary condition $e_w = 1, u_{st} = 0$. Points labelled (a–d) correspond to the four panels of figure 16.

With the energy-sink boundary condition, $e_w = 0.5$, our calculations were confined to smaller values of Δ/d and, over the range covered, Ω_r was found to increase with increasing Δ/d . However, had the calculations been extended to much larger plate separations, we suspect that the growth rate of the stationary mode would have passed through a maximum in the same way as described above.

The effect of changing $\bar{\nu}$ from 0.35 to 0.24, with the same value for Δ , can be seen by comparing figure 17 with figure 12. When $\bar{\nu}$ is decreased the positions of the peaks of the dominant stationary modes shift to markedly smaller values of K_x , by about the same amount for all three types of boundary condition, while the height of the peak is decreased for both the source and sink boundary conditions. The height changes very little for the adiabatic case.

An important general conclusion is that the forms of the dominant branches of eigenvalues remain similar on moving around the $(\bar{\nu}, d/\Delta)$ -plane. The only major qualitative change in behaviour occurs when the height of the peak of the stationary mode branch falls below the highest intercept of a branch of eigenvalues with the axis $K_x = 0$, and this triggers the switch to layering as the dominant mode of instability.

Finally, it is important to recognize the role of the inelasticity of collisions between

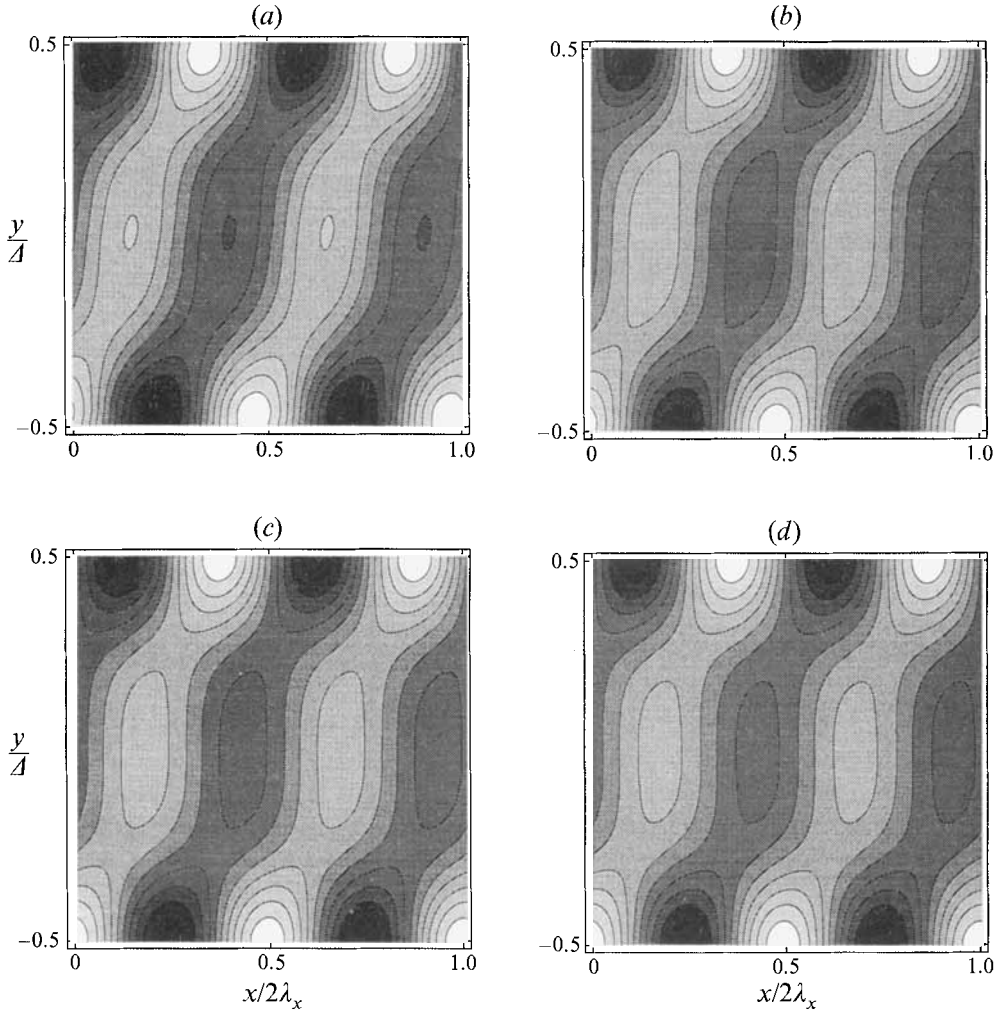


FIGURE 16. Eigenfunctions $v(x, y)$ for the conditions represented by the four points labelled (a–d) in figure 15. (a) $x/A = 13.2 x/2\lambda_x$, (b) $x/A = 26.9 x/2\lambda_x$, (c) $x/A = 53.9 x/2\lambda_x$, (d) $x/A = 109.3 x/2\lambda_x$.

particles in determining the nature of the dominant instability. Figure 18 reproduces the curves of figure 4, obtained with the sink boundary condition and $e_p = 0.8$, and supplements them with corresponding results for the same boundary conditions, but with both a larger (0.9) and a smaller (0.7) value for e_p . When $e_p = 0.9$ we found no dominant stationary mode with structure in the x -direction. The dominant mode is layering, with $K_x = 0$, and even this mode grows most slowly with this choice for e_p . When $e_p = 0.7$, on the other hand, the dominant stationary-mode peak is higher than in the base case, $e_p = 0.8$, and the layering mode also grows most quickly in this case, though it is by no means the dominant mode. These results indicate that the instability of the shear flow is a consequence of the inelasticity of particle–particle collisions; in particular, the strong stationary mode instability with structure in the x -direction appears only when the coefficient of restitution for these encounters is sufficiently small.

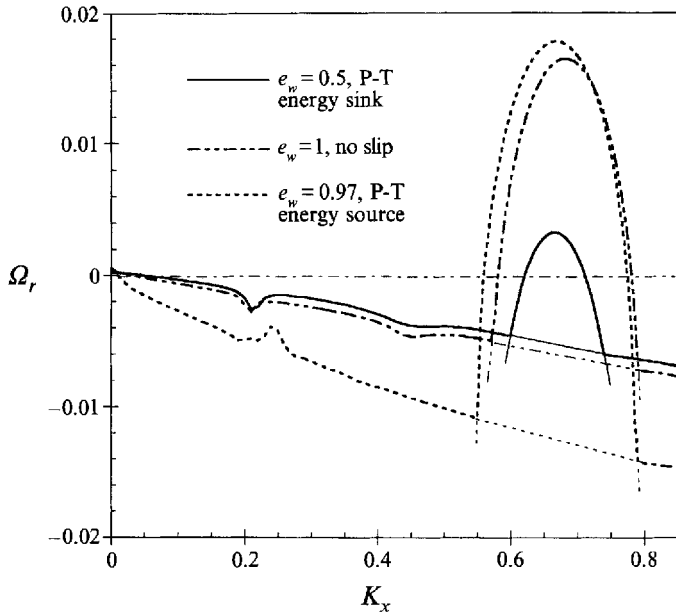


FIGURE 17. Effect on the leading modes of changing the value of $\bar{\nu}$. All conditions as for figure 12, with which the present figure should be compared, except that $\bar{\nu} = 0.24$.

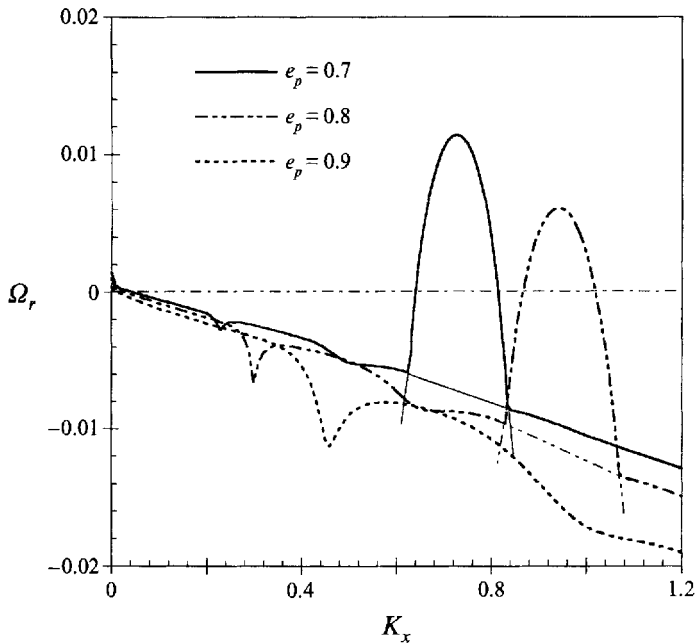


FIGURE 18. Effect on the leading modes of changing the value of e_p . $(\bar{\nu}, \Delta/d) = (0.35, 89)$. Parameter values as for figure 4, except that results are presented for three values of e_p , as indicated on the figure.

5. Unbounded plane shear

As noted above, equations (21)–(24) and the linearized small-perturbation equations derived from them can of course be used to examine the stability of an unbounded plane shear flow (see Savage 1992; Babić 1993; Schmid & Kytömaa 1993). Here we

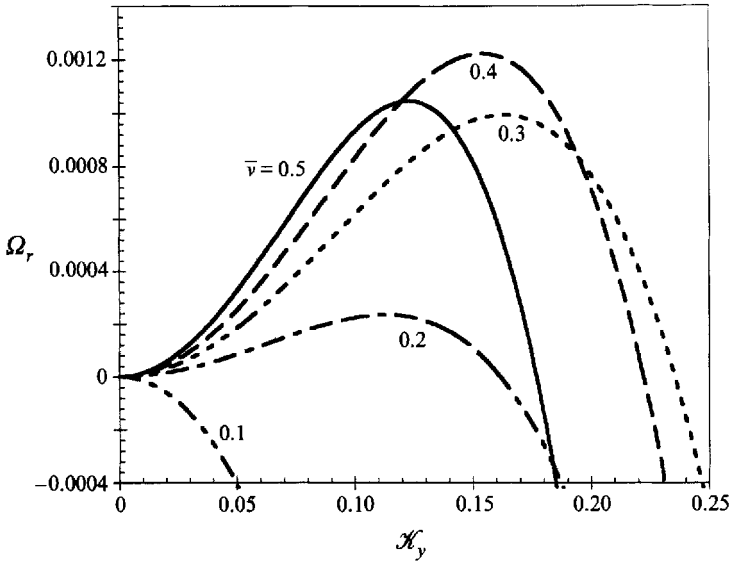


FIGURE 19. Dimensionless growth rate versus \mathcal{K}_y for the problem of unbounded shearing motion, with various values of \bar{v} , as indicated on the figure. Parameter values as in table 1.

shall address just two aspects of the unbounded flow problem: first, its relation to the stability problem for the bounded layer and, second, the effect of relaxing the constraint to two dimensions and permitting structure to develop in the z -direction (i.e. the direction of the vorticity).

As noted in the Introduction, among the perturbation modes that have been studied for the unbounded problem, only among those which are independent of x , and therefore represent ‘layering’ modes, can we find solutions which might be compatible with the boundary conditions of the bounded problem. A dimensionless growth rate Ω_r can be defined for these modes exactly as for the bounded case, using the shear rate of the base state as a scaling factor, and it depends on the volume fraction \bar{v} in the base state and the wavenumber k_y . The latter can no longer be scaled by the plate spacing, so instead we define a dimensionless wavenumber, scaled on the particle diameter, by $\mathcal{K}_y = k_y d$. Then with $e_p = 0.8$ the computed relation between Ω_r and \mathcal{K}_y , for various values of \bar{v} , is shown in figure 19. It is seen that the base state is stable when $\bar{v} = 0.1$ and, indeed, for all smaller values of \bar{v} , but for larger values the growth rate reaches a maximum positive value for some value of \mathcal{K}_y . This maximum growth rate is largest when $\bar{v} = 0.4$, so here the granular material is least stable to this form of perturbation. (As noted in the Introduction, these results contradict the conclusion of McNamara that unbounded shear flow is always stable.)

It is straightforward to extend this analysis to perturbations which do not depend on x but are allowed to depend on z , as well as y (see Babić 1993) since the linearized perturbation equations then have constant coefficients, and their solutions are harmonic in both y and z . The corresponding modes are again of the layering type, but now the layers are no longer normal to the y -axis; instead they are inclined so that their normal is in the direction of the vector $(\mathcal{K}_y, \mathcal{K}_z)$ in the (y, z) -plane. The analogue of figure 19 is then a set of contour maps of Ω_r in the $(\mathcal{K}_y, \mathcal{K}_z)$ -plane, one for each value of \bar{v} . Figure 20 is such a diagram, but in each panel we have plotted only the neutral stability contour, $\Omega_r = 0$. For $\bar{v} \geq 0.25$ the dominant mode, which grows most rapidly has $\mathcal{K}_z = 0$ and therefore represents layering of the sort encountered previously, with

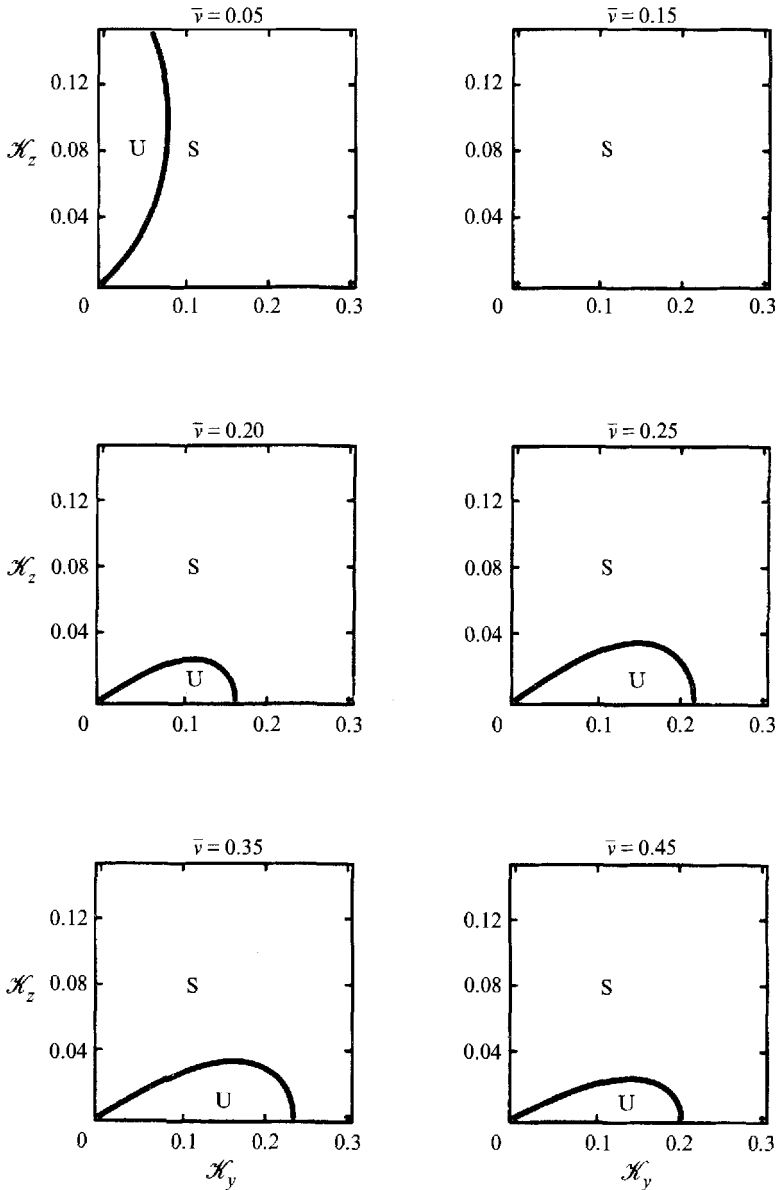


FIGURE 20. Domains of instability in the $(\mathcal{K}_y, \mathcal{K}_z)$ -plane for unbounded shearing motion at various values of \bar{v} , with disturbances permitted in the direction of the vorticity. *U* denotes unstable and *S* stable.

the layers parallel to the (x, z) -planes. The base state becomes completely stable when \bar{v} is reduced to 0.15. However, it becomes unstable again for still smaller values of \bar{v} , but the orientation of the dominant layering instability has changed and the layers are now parallel to the (x, y) -plane, with normal in the direction of the vorticity. This curious behaviour appears to have escaped notice in the works on the unbounded problem referred to above.

We turn now to the relation between the results for the unbounded shear flow and those for shear of a layer bounded by solid plates. This is best seen by focusing on the adiabatic case for the bounded shear layer. Then we expect the layering modes in the

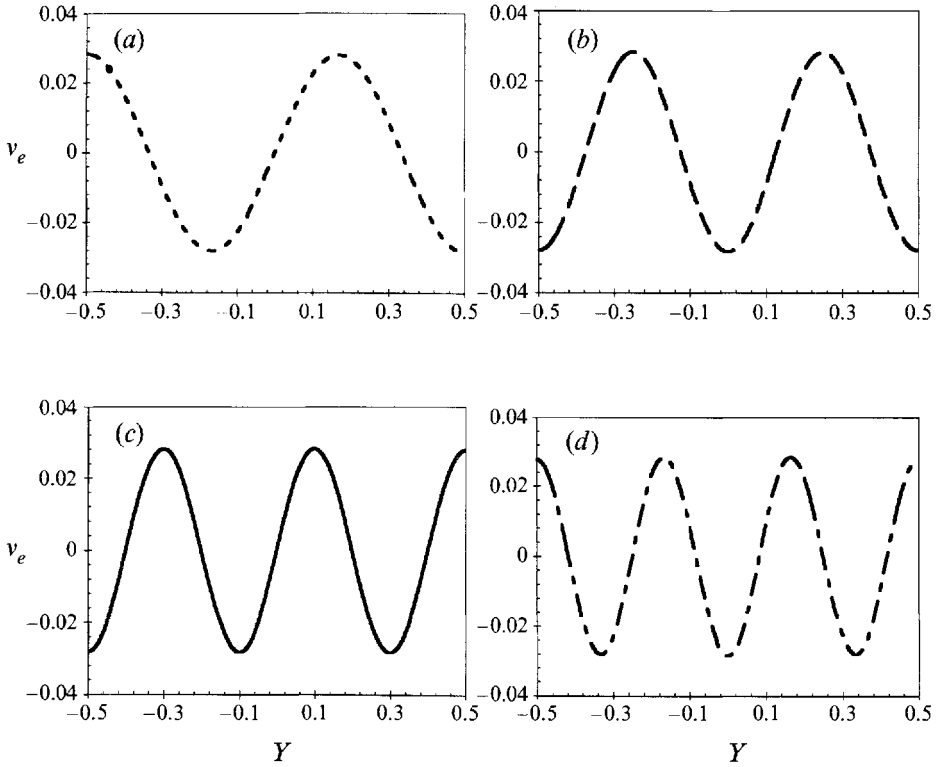


FIGURE 21. Harmonic eigenfunctions $v_e(Y)$ for the adiabatic case at $(\bar{v}, \Delta/d) = (0.35, 89)$. Parameter values as for figure 3, except that wall boundary conditions are changed to $e_w = 1$, $u_{st} = 0$, the adiabatic case. (a), (b), (c) and (d) represent successively higher harmonics.

bounded problem to coincide with certain selected layering modes of the unbounded problem. This follows since bounded layers can be stacked, with the centreline velocity for the base state increased by an increment of u_1 for each successive layer and, as the number of layers assembled in this way increases without bound, a viable mode for the unbounded problem is generated. Not all possible layering modes of the unbounded problem can be generated in this way, since K_y is constrained by the boundary conditions to take one of a discrete set of values in the bounded problem.

These considerations are illustrated in figure 21, where the eigenfunctions $v_e(Y)$ are plotted for the four most rapidly growing layering modes of the bounded problem with adiabatic boundary conditions and $(\bar{v}, \Delta/d) = (0.35, 89)$. Each of these modes is harmonic in Y , and can therefore be characterized by a dimensionless wavenumber K_y , which can in turn be re-scaled to match the scaling of the unbounded problem, writing $\mathcal{K}_y = K_y d/\Delta$. Then in figure 22 points (a), (b), (c) and (d) represent $(\Omega_r, \mathcal{K}_y)$ for these four modes of the bounded problem, superimposed on the curve relating Ω_r to \mathcal{K}_y for the corresponding unbounded problem. The relation is plain. The small displacement of points (c) and (d) from the curve is merely a measure of the computational error in the algorithm for determining the eigenvalues of the bounded problem.

The dominant stationary modes for the bounded problem, with structure in the x -direction, are not related in any such simple way to modes of the unbounded problem, even in the adiabatic case. Unlike the layering modes they cannot be stacked to generate a solution of the unbounded problem, since the whole pattern of particle concentration perturbations (see figure 13) is stationary relative to the material in the

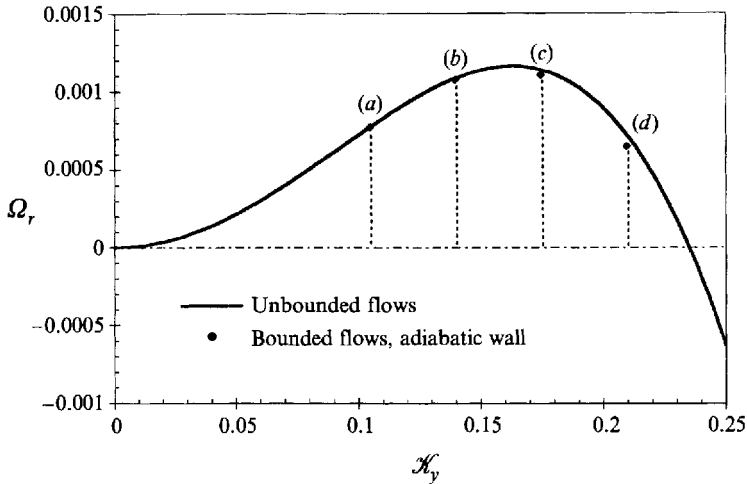


FIGURE 22. Points corresponding to the conditions (a), (b), (c) and (d) of figure 21 superimposed on a plot of Ω_r versus \mathcal{K}_y for the corresponding problem of unbounded shearing motion.

central plane. Consequently, if successive layers with centreline particle velocities incremented by u_1 are stacked to generate an unbounded plane shear field in the base state, discontinuities are created in the phase velocity of the perturbation pattern at their junctions. Thus these modes, which dominate the behaviour of perturbations for the bounded problem over a wide region of its parameter space, have no analogue in the unbounded problem.

6. Conclusions

Bounded shear flow is found to be unstable only when collisions between the particles are sufficiently inelastic. For given particles, and bounding walls of given structure, the stability is determined by the values of two parameters, namely the mean volume concentration of the particles in the layer, and the ratio of the plate separation to the particle diameter. The rate of shear plays no part in locating the stability boundary, but for points not on that boundary the rate of growth or decay of perturbations is proportional to the rate of shear. The sheared layer is stable when it is sufficiently thin and becomes unstable as the thickness is increased to a value which depends on the mean particle concentration.

The dominant instabilities take one of two forms: either relatively slow growing layers of alternating high and low particle concentration parallel to the planes of shear, or faster growing, more complicated stationary patterns with structure in the direction of flow. Though the former are closely related to corresponding instabilities of unbounded shear flow, the latter have no analogue in the unbounded problem. They consist of a pattern of three layers of regions of alternating higher and lower particle concentration, one on the centreplane and one near each wall, with the regions aligned in inclined bands of three. The direction of inclination conforms with the direction of shear, but the angle of inclination is unaffected by the rate of shear. If these patterns are plotted with the coordinate in the direction normal to the shear planes scaled by the thickness of the shear layer, and the coordinate in the direction of flow scaled by their wavelength in that direction, their geometry appears to be remarkably insensitive to the physical properties of the particles and the bounding walls, and to the thickness of the layer and the mean concentration of particles. Thus, they seem to owe their

existence merely to the presence of impenetrable walls bounding the shearing layer. It should be emphasized that they are not the same as the patterns of clusters of increased density seen in dynamic simulations of *unbounded* shear flow. The clusters seen in simulations convect with the shear field whereas these patterns are fixed in space, so the regions of increased density are in no sense clusters of identifiable particles; indeed, the particles are continually convected through regions of both high and low density.

Clusters which convect with the material are seen in the present work. They occur in the leading mode when this is a travelling wave. However, they have negative growth rates except at very long wavelengths, when they grow slowly, but are elongated so much in the direction of shear that they bear little geometric resemblance to the clusters reported in simulations. However, it is possible that convecting clusters of shorter wavelength, though formally stable, might have large transient amplification as found by Schmid & Kytömaa (1994) for the case of unbounded shear. This could explain their appearance in simulations as transient phenomena triggered by a small random perturbation, rather than true instabilities. An extension of the analysis of Schmid & Kytömaa to the bounded shear layer would, therefore, be interesting.

An investigation of the dynamic behaviour of *bounded* shear layers by direct dynamical simulation and comparison with the predictions of the continuum equations presented here, particularly those relating to the dominant stationary mode, might provide a valuable test of the validity of the approximations leading to the continuum equations.

This work has been supported by the National Science Foundation under grant number CTS 92-07469. R.J. also thanks Trinity College, Cambridge, for an appointment as a Visiting Fellow Commoner, and the Department of Applied Mathematics and Theoretical Physics, Cambridge University for use of its facilities during the later stages of the work.

REFERENCES

- BABIĆ, M. 1993 On the stability of rapid granular flows. *J. Fluid Mech.* **254**, 127–150.
- GALLAGHER, A. P. & MERCER, A. MCD. 1962 On the behaviour of small disturbances in plane Couette flow. *J. Fluid Mech.* **13**, 91–100.
- GOLDHIRSCH, I., TAN, M.-L. & ZANETTI, G. 1993 A molecular dynamical study of granular fluids I: the unforced granular gas in two dimensions. *J. Sci. Comput.* **8**, 1–40.
- HAFF, P. K. 1983 Grain flow as a fluid-mechanical phenomenon. *J. Fluid Mech.* **134**, 401–430.
- HOPKINS, M. A. & LOUGE, M. Y. 1991 Inelastic microstructure in rapid granular flows of smooth disks. *Phys. Fluids A* **3**, 47–57.
- JENKINS, J. T. 1987 Rapid flows of granular materials. In *Non-Classical Continuum Mechanics*, pp. 213–225. Cambridge University Press.
- JENKINS, J. T. & RICHMAN, M. W. 1986 Boundary conditions for plane flows of smooth, nearly elastic, circular disks. *J. Fluid Mech.* **171**, 53–69.
- JENKINS, J. T. & SAVAGE, S. B. 1983 A theory for the rapid flow of identical, smooth, nearly elastic, spherical particles. *J. Fluid Mech.* **130**, 187–202.
- JOHNSON, P. C. & JACKSON, R. 1987 Frictional-collisional constitutive relations for granular materials, with application to plane shearing. *J. Fluid Mech.* **176**, 67–93.
- LUN, C. K. K., SAVAGE, S. B., JEFFREY, D. J. & CHEPURNIY, N. 1984 Kinetic theories for granular flow; inelastic particles in Couette flow and slightly inelastic particles in a general flow field. *J. Fluid Mech.* **140**, 223–256.
- MCNAMARA, S. 1993 Hydrodynamic modes of a uniform granular medium. *Phys. Fluids A* **5**, 3056–3070.

- MELLO, T. M., DIAMOND, P. H. & LEVINE, H. 1991 Hydrodynamic modes of a granular shear flow. *Phys. Fluids A* **3**, 2067–2075.
- MOFFATT, H. K. 1967 The interaction of turbulence with strong wind shear. In *Atmospheric Turbulence and Radio Wave Propagation* (ed. A. M. Yaglom & V. I. Tatarsky), pp. 135–156. Moscow: Nauka.
- RICHMAN, M. W. 1988 Boundary conditions based upon a modified Maxwellian velocity distribution for flows of identical, smooth, nearly elastic spheres. *Acta Mechanica* **75**, 227–240.
- SAVAGE, S. B. 1992 Instability of unbounded uniform granular shear flow. *J. Fluid Mech.* **241**, 109–123.
- SCHMID, P. J. & KYTÖMAA, H. K. 1994 Transient and asymptotic stability of granular shear flow. *J. Fluid Mech.* **264**, 255–275.
- THOMSON, W. 1887 Stability of fluid motion. Rectilineal motion of viscous fluid between two parallel planes. *Phil. Mag.* **24** (August), 188–196.
- WANG, C.-H. 1995 Instabilities in granular material flows. PhD dissertation, Princeton University.